Title
Regional scale probabilistic procedure for estimating lateral spread displacements

Authors
Bain, Christopher A
Bray, Jonathan D

Publication Date
2023-08-01

DOI
10.1016/j.soildyn.2023.107928

Peer reviewed

Soil Dynamics and Earthquake Engineering 171 (2023) 107928

Contents lists available at ScienceDirect

Soil Dynamics and Earthquake Engineering

journal homepage: www.elsevier.com/locate/soildyn

Regional scale probabilistic procedure for estimating lateral spread displacements

Christopher A. Bain *, Jonathan D. Bray

Dept. of Civil and Environ. Eng., Univ. of California, Berkeley, USA

ARTICLE INFO

Keywords:
Liquefaction
Lateral spreading
Probabilistic
Regional assessment
Seismic displacement

ABSTRACT

Regional scale liquefaction assessments are currently performed using approaches such as qualitative liquefaction susceptibility rankings based on mapped geology and groundwater information, interpolation of liquefaction vulnerability indices from widely spaced subsurface explorations, or use of proxies for geologic, geotechnical, and groundwater conditions that affect liquefaction triggering calculations. These methods often do not include assessments of the consequences of liquefaction, such as the potential lateral spread displacement and its uncertainty. This study presents a procedure for probabilistically assessing liquefaction-induced lateral spread displacement at the regional scale by estimating a distribution of lateral displacement index (LDI) using models conditioned on surficial geology, depth to groundwater, peak ground acceleration, and earthquake magnitude. Existing topographic correlations are used to convert distributions of LDI to distributions of lateral spread displacement. Case histories illustrate its performance in regional assessments of the lateral spread hazard.

1. Introduction

Liquefaction-induced lateral spread displacement is a common mechanism of seismic displacement and often causes severe damage to port facilities and distributed infrastructure, such as buried pipelines. The lateral spread displacement hazard can be assessed at the site-specific scale using empirically-based, in-situ penetration test methods or by performing advanced numerical analyses that requires laboratory testing, but these methods are impractical for assessing potential lateral spread displacements across large, distributed infrastructure systems. Distributed infrastructure systems such as water and gas pipeline networks may include hundreds of kilometers of pipelines, and the liquefaction and lateral spread displacement hazard may vary significantly throughout the geographic area of these networks. To assess the lateral spread displacement hazard to lifeline systems, a need exists for improved regional scale analysis methods. This paper describes and illustrates the use of a new procedure to probabilistically assess potential liquefaction-induced lateral spread displacements at regional scales.

The procedure proposed in this paper was developed as part of a larger research effort to create a new seismic risk assessment program called *OpenSRA*, which utilizes the Pacific Earthquake Engineering Research (PEER) center's Performance-Based Earthquake Engineering (PBEE) methodology. The PEER PBEE framework assesses seismic performance at the system level by probabilistically quantifying an intensity measure (IM), such as the peak ground acceleration (PGA), and the response of the system to the IM in terms of seismic displacement or other engineering demand parameters (EDP). The EDPs are used with fragility relationships to estimate the damage to the system such as longitudinal pipe strain or other damage measures (DM). Finally, the DMs are used to evaluate decision variables (DV) such as the probability of pipeline rupture. To be used in the PBEE framework for estimating the seismic displacement EDP, the proposed method is required to estimate quantitatively potential lateral spread displacement and the uncertainty of its estimate. The method is intended for regional scale analyses for the purpose of identifying areas of high lateral spread displacement hazard where site-specific techniques can further refine the lateral spread displacement hazard.

To develop the procedure, cone penetration test (CPT) data are collected in a region and are sorted by surficial geology. The lateral displacement index (LDI) is calculated for each CPT for 225 unique combinations of depth to groundwater (GWT), peak ground acceleration (PGA), and earthquake moment magnitude (M_w). Standard penetration test (SPT) data could also be used to inform the models, albeit with greater uncertainty and lower reliability in comparison to the CPT. The data are used to derive relationships to estimate the probability that LDI equals zero ($P_{LDI=0}$), where small values of LDI are assumed to be

* Corresponding author.
E-mail addresses: chris_bain@berkeley.edu (C.A. Bain), jonbray@berkeley.edu (J.D. Bray).

https://doi.org/10.1016/j.soildyn.2023.107928
Received 19 December 2022; Received in revised form 18 February 2023; Accepted 22 March 2023

essentially zero, and the mean, non-zero LDI. The $P_{LDI=0}$ and mean, non-zero LDI relationships are combined using a mixed-random variable model whereby there is a mass probability that LDI equals zero (denoted LDI_0) and a continuous distribution of non-zero LDI. The distribution of non-zero LDI is then converted to a distribution of non-zero lateral spread displacement using existing topographic correlations of LDI to lateral spread displacement. Finally, to realistically model the spatial extent of lateral spreading, the modeled lateral displacements are scaled by the proportion of a surficial geologic unit estimated to be susceptible to surface liquefaction and a minimum displacement threshold is established. The modeling is shown to estimate reasonably both the spatial extent and severity of lateral spreading in the San Francisco Bay Area of California for the 1989 M_w 6.9 Loma Prieta earthquake and in Christchurch, New Zealand for the 2010 M_w 7.1 Darfield and 2011 M_w 6.2 Christchurch earthquakes.

2. Available regional scale liquefaction triggering and lateral spread displacement procedures

Evaluating liquefaction triggering and potential lateral spread displacements at regional scales is challenging due to the variability and large uncertainty inherent to estimating geotechnical, groundwater, and topographic conditions as well as the earthquake shaking intensity. The Zhu et al. [1,2] procedures use proxies for geotechnical and groundwater conditions, such as slope-based shear wave velocity in the upper 30 m (V_{S30}), compound topographic index (CTI), mean annual precipitation, and distance to the coast, nearest river, or nearest body of water, along with the PGA or peak ground velocity (PGV) to estimate the probability of liquefaction triggering. Given that these procedures use only proxies for subsurface conditions, their estimates are highly uncertain. Moreover, these methods do not quantify the aleatory variability (uncertainty due to inherent randomness) or epistemic uncertainty (uncertainty due to lack of data). Furthermore, the Zhu et al. methods [1,2] do not attempt to quantify the potential consequences of liquefaction, such as lateral spread displacements.

Alternatively, geologic-based assessments [3] have been employed for decades to qualitatively assess the relative susceptibility of surficial geologic units to liquefaction triggering over regions with large-scale geologic mapping that differentiates quaternary units by age and depositional environment. Geologic-based maps of relative liquefaction susceptibility can be converted to quantitative estimates for the probability of liquefaction triggering and lateral spread displacement using the Hazus [4] methodology. The Hazus method [4] for estimating lateral spread displacement is based on the liquefaction severity index (LSI) [5], which loosely correlates the severity of liquefaction to the distance to the seismic energy source (R) and the earthquake M_w. The Hazus method implicitly assumes that lateral spreading is only an inertia driven process, whereby the stronger the shaking, the greater the lateral spread displacement, and it does not consider topography in estimating displacements. This approach does not consider the potential mechanism for lateral spread displacement where earthquake shaking generates excess pore water pressure resulting in liquefaction and overlying, non-liquefied sediments move gently downslope or towards a free-face due largely to gravitational forces greater than the strength of the liquefied material at times with high excess pore water pressures. For these reasons, the Hazus method may not reliably characterize the lateral spread displacement hazard. In addition, Hazus does not estimate the aleatory variability or epistemic uncertainty in the lateral spread displacement estimate.

Another approach to evaluating liquefaction at regional scales is to calculate liquefaction vulnerability indices, such as the liquefaction potential index (LPI) [6] or the liquefaction severity number (LSN) [7], at CPT locations or at soil exploratory borings with standard penetration test (SPT) blow counts, to then interpolate between investigation sites using kriging techniques, and lastly, to correlate the calculated vulnerability index to the probability of liquefaction triggering or potential consequences of liquefaction. This approach has validity but is limited to areas with many geotechnical investigations spaced relatively close together. It is difficult to apply these techniques in seismic risk analyses, which may require evaluating thousands of ground shaking iterations, and it is difficult to track the uncertainty from dozens to thousands of individual geotechnical investigations.

A recent paper by Paolella et al. [8] proposed a unitless, generalized liquefaction severity number (GLSN) to estimate liquefaction severity at regional scales. Their method calculates a modified LDI with a newly proposed depth weighting factor which uses the inverse tangent function. The modified LDI is then multiplied by a topography factor (TF) based on the topographic correlations presented by Zhang et al. [9]. The GLSN is calculated at individual CPTs across a study region and interpolated using kriging techniques. Liquefaction severity is assessed qualitatively by binning the GLSN into broad categories such as no damage, minor damage, moderate damage, and severe damage. While this method is reasonable for assessing general categories of potential liquefaction-induced damage, it does not provide an estimate of potential lateral spread displacement or assess the uncertainty of the displacement estimate. The PBEE framework employed in the PEER project described previously requires this information.

In another approach that was the inspiration of this paper, Holzer et al. [10] merged geologic-based evaluations with subsurface geotechnical investigations to develop what they termed *Liquefaction Probability Curves for Surficial Geologic Deposits*. Holzer et al. [10] collected CPTs in several study regions, sorted them by surficial geology, and calculated LPI for many different PGAs and for two groundwater depths (1.5 and 5 m). PGA was scaled by the magnitude scaling factor (MSF) from Youd et al. [11] to generalize the relationships to all earthquake magnitudes and at each value of the magnitude-scaled PGA, the percentage of CPTs within a geologic unit with LPI >5 is taken to be the probability of liquefaction. The threshold LPI value of 5 was selected because Toprak & Holzer [12] found that liquefaction is likely when LPI >5. Logistic models were then fitted to the data to create relationships that estimate the probability of liquefaction triggering given magnitude-scaled PGA and depth to groundwater of 1.5 or 5 m.

While the Holzer et al. [10] method was a significant contribution to advance regional scale modeling techniques, it is not without limitations. Holzer et al. [10] presents models for two discrete groundwater depths (1.5 and 5 m) rather than modeling the depth to groundwater as a continuous variable. The method also employs LPI, which has validity in estimating the likelihood of surface manifestations of liquefaction (i.e., ground failure), but LPI has not been correlated directly to lateral spread displacement (LD). Finally, Holzer et al. [10] do not estimate aleatory variability or epistemic uncertainty with their method.

3. Topographic drivers of lateral spreads and the lateral displacement index

As discussed previously, lateral spread displacement is often driven by gravitational forces as non-liquefied soils overlying liquefied sediments move gently downslope or towards a free-face (e.g., river banks or the waterfront at port facilities). In other cases, inertial effects may also contribute to lateral spread displacements; however, the liquefaction of continuous soil layers is still a primary mechanism of lateral spreading in these cases. Methods for estimating potential lateral spread displacements typically require site-specific geotechnical investigations (e.g. Refs. [9,13–15], and characterize in-situ static driving stresses using topographic slope or free-face ratio (*FFR*, which is the ratio of the distance to the bottom of a free-face feature, *L*, to the height of the free-face, *H*). The Zhang et al. [9] procedure is one of the most commonly employed CPT-based methods in engineering practice. Its topographic correlations for converting LDI to LD are used in this study.

Zhang et al. [9] correlates LDI to lateral spread displacement (LD) for gently sloping sites far from a free-face as Equation (1) and the correlation for sites near a free-face is presented as Equation (2).

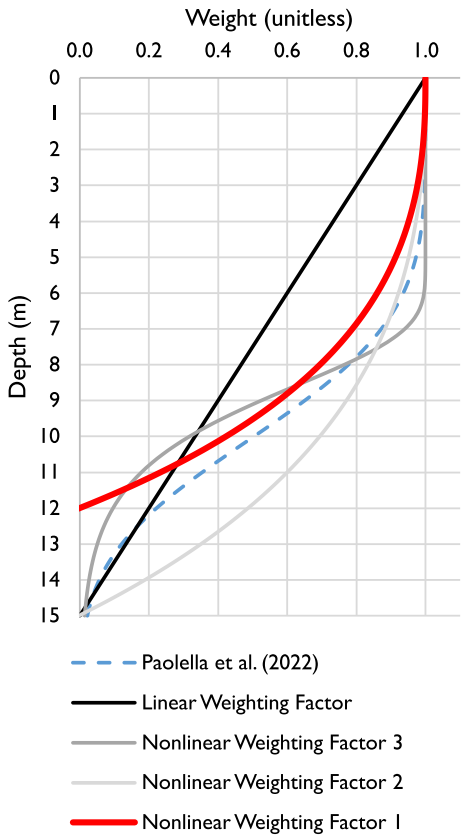

Fig. 1. (color): Investigated depth weighting factors (DWFs) with selected DWF in red.

$$\frac{LD}{LDI} = S + 0.2 \quad for\ 0.2\% < S < 3.5\% \tag{1}$$

$$\frac{LD}{LDI} = 6 * (FFR)^{-0.8} \quad for\ 4 < FFR < 40 \tag{2}$$

where S is the topographic slope in percent and FFR is the free-face ratio (L/H). LDI as defined by Zhang et al. [9] is calculated using Equation (3) and is an index of the cumulative shear strain potential from all liquefiable layers in the subsurface.

$$LDI = \int_0^{z_{max}} \gamma_{max} dz \tag{3}$$

The maximum potential shear strain of a soil layer, γ_{max}, is a function of the relative density of the soil layer and the excess pore pressure ratio, represented by the factor of safety against liquefaction triggering (FS_{Liq}). For this study, the factor of safety against liquefaction triggering was estimated using the 50% probability of liquefaction cyclic resistance ratio (CRR) relationships from Boulanger & Idriss [16] and the Ku et al. [17] probabilistic modification to the Robertson & Wride [18] as updated by Robertson [19] procedure, giving equal weight to the two methods. As recommended by Holzer et al. [10], soils in the San Francisco Bay Area with soil behavior type index $I_c \geq 2.4$ were considered not susceptible to liquefaction triggering. For soils in Christchurch, soils with $I_c \geq 2.6$ were assumed to not be susceptible to liquefaction triggering, which is a typical assumption (e.g., Maurer et al. [20]). To evaluate liquefaction triggering using Boulanger & Idriss [16], their relationship to estimate the fines content was used for soils in the San Francisco Bay Area while the relationship from Maurer et al. [20] was used to estimate the fines content for soils in Christchurch. Relative density was estimated using the relationships from Idriss & Boulanger, Jamiolkowski et al., and Kulhawy & Mayne [21–23], giving weights of 0.4, 0.3, and 0.3, respectively. γ_{max} was calculated using the relationships from Zhang et al. and Idriss & Boulanger [9,21], giving equal weight to the two methods.

Table 1
Range of investigated parameters.

Parameter	Range of Values
PGA (g)	0.1, 0.15, 0.2, 0.3, 0.4, 0.5, 0.6, 0.8, 1.0
M_w	6.0, 6.5, 7.0, 7.5, 8.0
GWT (m)	0.5, 1.5, 3.0, 5.0, 7.0

The definition of LDI presented in Equation (3) assumes liquefaction at all depths contributes equally to lateral displacement at the ground surface, with the only recommended limitation from Zhang et al. [9] being that liquefaction triggering should not be evaluated below a depth of 23 m. In the regions evaluated for this study, free-faces are generally small (typically a few meters) so estimating lateral spread displacement by considering liquefaction triggering to a depth of 23 m leads to significant overestimation of the lateral spread hazard for the free-face condition. Additionally, for the gently sloping ground condition, liquefaction at depths greater than about 10–15 m is unlikely to contribute to lateral displacement at the ground surface. For these reasons, a sensitivity study was performed to estimate an appropriate maximum depth for evaluating liquefaction triggering and to investigate potential depth weighting factors (DWFs) to limit the contribution of deep liquefiable layers to the lateral spread hazard.

It became clear early in the study that a DWF was required to capture the observed lateral spread displacements in the 1989 Loma Prieta earthquake. LDI was calculated with no DWF to maximum depths of 10 m and 15 m, and using several potential forms of DWFs, which are presented in Fig. 1. The linear DWF is similar to that employed in the calculation of LPI, but the linear DWF used to calculate LPI is linear to 20 m and not 15 m. DWF 1 and DWF 2 place more weight on liquefied layers near the ground surface compared to the linear DWF, and apply zero weight on liquefiable layers below 12 m and 15 m, respectively. DWF 3 is similar to that recommended independently by Paolella et al. [8]. The intent of DWF 3 is to place most weight on the upper 7 m of the soil profile and little weight to soil below a depth of 12 m with a sharp transition.

To evaluate the appropriateness of each of these assumptions, the procedure described in later sections of this paper was evaluated in the San Francisco Bay Area for the M_w 6.9 Loma Prieta earthquake and the results interrogated. It was found that evaluating LDI with no DWF leads to unacceptable overestimation of the spatial extent of lateral spreading and displacement magnitudes. DWF 1 (bolded red in Fig. 1) reduces the overestimation of the lateral spread hazard at the regional scale to an appropriate degree for the San Francisco Bay Area dataset. DWF 1 also worked well for the Christchurch dataset, which will be discussed later. DWF 1 was developed to place the most weight on the upper 6 m of the soil profile with no weight for soils below a depth of 12 m, which is consist with the patterns of lateral spread ground deformation observed in the field. There is epistemic uncertainty in the form of the DWF, and several DWFs could be included using a logic tree approach. However, in this study DWF 1 worked best in this regional scale method to reduce the overestimation of the lateral spread hazard due to deep liquefiable layers so it was adopted. Accordingly, the definition of LDI is modified in this study to incorporate DWF 1 as presented in Equation (4).

$$LDI = \int_0^{z_{max}} \gamma_{max} w(z) dz, \quad where\ w(z) = 1 - \sinh\left(\frac{z}{13.615}\right)^{2.5} \tag{4}$$

In addition to incorporating DWF 1 in the calculation of LDI, LDI was assumed to be zero for CPTs with less than 0.30 m of soil expected to liquefy (i.e., soil profile had less than 0.30 m with $FS_{Liq} < 1.0$). For lateral spreading to occur, liquefied soils must be continuous over a relatively large area, which is less likely when only thin layers of liquefied soil are present. The selected value of 0.3 m is still likely

conservative as the thinnest liquefied layer in the case history database used by Youd et al. [13] to develop their lateral spread displacement procedure was 1.0 m and the thinnest liquefied layer in the case histories used by Zhang et al. [9] to develop their procedure was 0.6 m. LDI was calculated for each of the CPTs for every combination of PGA, M_w and GWT presented in Table 1 (225 unique combinations).

4. Data sources and uncertainty

The following subsections summarize the datasets available in the two study regions evaluated in this paper and discuss and quantify their uncertainty. While the aleatory variability and epistemic uncertainty in each dataset could be evaluated using Monte Carlo or other error propagation techniques, only the aleatory variability in the assessment of LDI and the aleatory variability in the PGA are assessed in this study. By evaluating the plus- and minus-one standard deviation LDI and PGA values, their sensitivity to the overall lateral spread displacement assessment are demonstrated. A full probabilistic study that propagates the uncertainty in each of the datasets could be performed, but the purpose of this paper is to introduce and validate the new method. The new method is incorporated within the *OpenSRA* software, which will be used to perform a comprehensive seismic risk assessment in regions within California.

4.1. San Francisco Bay Area datasets and uncertainty

The implementation of the proposed regional scale liquefaction-induced lateral spread displacement procedure is illustrated through its use in two regions: the San Francisco Bay Area of California and the Christchurch area of New Zealand. In the San Francisco Bay Area, the CPT database comes from the United States Geological Survey (USGS) [24], the geologic map is the 1:24,000 scale mapping from Witter et al. [25]; and a groundwater table model assuming local mean sea level (LMSL) conditions comes from the USGS Coastal Storm Modeling System (CoSMoS) project [26], who modeled the depth-to-groundwater in the coastal areas around the San Francisco Bay Area using the groundwater modeling program MODFLOW [27]. Topographic slope and free-face ratio are derived from 10-m resolution digital elevation models (DEMs) of terrestrial elevations from the USGS [28] and a 10-m resolution DEM with bathymetric elevations of the San Francisco Bay from the USGS [29]. Geometry of free-face features in the Bay area comes from the Bay Area Aquatic Resources Inventory (BAARI) GIS database published by the San Francisco Estuary Institute and Aquatic Science Center [30] and from a shapefile database of streams in the San Francisco Bay Area published by the Bay Area Open Space Council [31]. The model is evaluated using the USGS *ShakeMap* estimates for the median PGA for the 1989 M_w 6.9 Loma Prieta Earthquake [32] and observations of liquefaction primarily from the USGS study [33] supplemented by those from the Seed et al. [34] study.

The datasets used for modeling in the San Francisco Bay Area all have uncertainty. Most of the CPTs in this dataset are electric cones but some are mechanical cones. CPTs have uncertainty in the measured corrected tip resistance (q_t) and the measured sleeve friction (f_s). Kulhawy & Mayne [23] estimate the coefficient of variation (COV) for tip resistance measurements collected with mechanical or electric cones is 10% and 5%, respectively. The COV for sleeve friction measurements collected with mechanical or electric cones is 20% and 10%, respectively. In addition to the uncertainty in the actual CPT tip resistance and sleeve friction measurements, interpreting CPT data introduces additional uncertainty into the assessment. For example, CPT measurements are used to estimate the fines content (FC) of potentially liquefiable sands in liquefaction triggering assessments with significant uncertainty. The variability in the tip resistance and sleeve friction measurements and the uncertainty associated with estimating fines content from CPT measurements were not considered in this study. Instead, measured values were used. However, a full probabilistic study could be performed with a logic tree approach to capture these sources of epistemic uncertainty.

The most significant potential uncertainty in the Witter et al. [25] mapping is in the accuracy of the mapped units. There is the potential that the units indicated on the map may not always align with the geology at the site. For the purposes of this study, all mapped units are assumed to be accurate.

The depth to groundwater model used in this study from the USGS CoSMoS project [26] has significant uncertainty which stems largely from the methods used to generate the model using MODFLOW [27]. There is also uncertainty due to the inherent temporal variability in the groundwater table. According to Befus et al. [35], the area's hydrogeology was modeled with uniform aquifer thickness along the coast with a horizontal impermeable layer at a depth of 50 m below sea level. Given that the properties of the aquifer are unknown, the aquifer hydraulic conductivity (k) was assumed to be constant with values of 0.1, 1, and 10 m/day assumed to span the estimated range of aquifer hydraulic conductivities in the study region. Depth to groundwater models were generated by solving the steady-state groundwater flow equation at a 10-m resolution. Model depth to groundwater estimates were compared to well measurements in the study area with the model assuming $k = 1$ m/day producing results that adequately approximate mean depth to groundwater conditions with the assumption of local mean sea level (LMSL) conditions. The models assuming $k = 0.1$ and 10 m/day systematically bias the model to produce high and low depth to groundwater estimates, respectively. The steady-state depth to groundwater model residuals assuming LMSL and $k = 1$ m/day is estimated to have COV $\approx$ 41% and it is assumed to be approximately lognormally distributed. The form of the residual distribution was not investigated by Befus et al. [35].

According to Wechsler [36], DEMs may be subject to three types of errors: blunders associated with the data collection process, systematic errors associated with improperly calibrated equipment or data processing software, and random errors. The USGS can identify and remove blunders and systematic errors, but random errors persist in the published datasets. According to Stoker & Miller [37], the uncertainty in the USGS 10-m DEMs is normally distributed with standard deviation equal to 0.82 m. This standard deviation was estimated using 10-m DEMs from all over the United States and may or may not accurately reflect the uncertainty of the 10-m DEMs in the Bay Area. These errors carry through the calculation of the topographic slope and the free-face ratio, but for the purposes of this study, the uncertainty in the calculated slope and free-face ratio resulting from the uncertainty in the DEM elevations was not considered.

ShakeMap provides estimates of the intensity of ground motions for the 1989 M_w 6.9 Loma Prieta earthquake as an uncertainty-weighted average of direct ground motion observations and estimates from ground motion models (GMMs). Total uncertainty is geospatially variable and is a function of the uncertainty obtained using a distance-to-observation spatial correlation function and the uncertainty of the GMMs. *ShakeMap* datasets for the Loma Prieta earthquake including uncertainty are available from the USGS [32]. For the purposes of this study, the lateral spread displacement model was evaluated using the median ground motion estimates and the sensitivity to the shaking intensity was interrogated by evaluating the model for the 16% and 84% probability of exceedance ground motion estimates.

The Witter et al. [25] geologic map for the San Francisco Bay Area was simplified into three distinct groups: the artificial fill over Holocene estuarine mud (*afem*) deposits, latest Holocene alluvial fan levee (*Qhly*) and similar highly susceptible alluvial and fluvial deposits, and Holocene alluvial fan (*Qhl*) and similar moderately susceptible alluvial and fluvial deposits. The USGS CPT database [24] does not contain enough CPTs in older deposits to attempt to estimate a distribution of LDI in those units. They are assumed to not be susceptible to liquefaction in this study. The USGS CPTs in the San Francisco Bay Area used in this study are overlaid on the simplified version of the Witter et al. [25] geologic

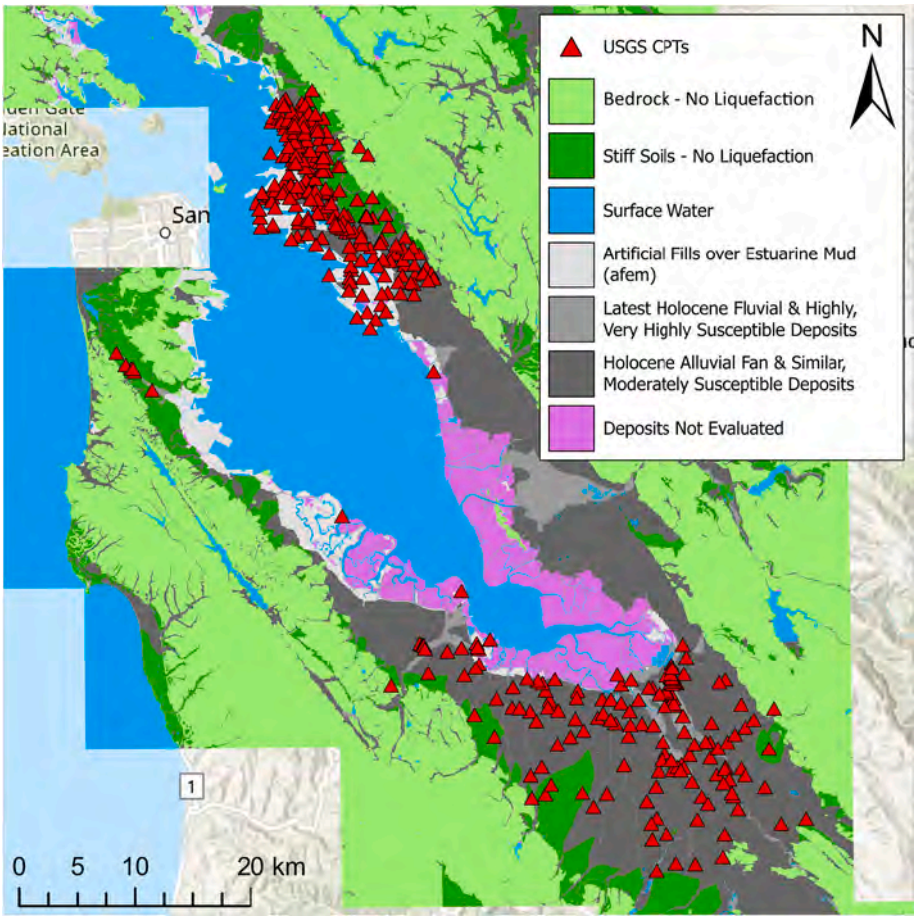

Fig. 2. (color): Locations of USGS CPTs in the San Francisco Bay Area overlaid on simplified version of the Witter et al. [25] geologic map.

Table 2
Number of CPTs in each investigated surficial geologic deposit.

Area	Surficial Geologic Deposit	Number of CPTs
San Francisco Bay Area	Artificial Fill over Estuarine Mud Deposits (*afem*)	89
	Latest Holocene Alluvial Fan Levee Deposits (*Qhly*)	41
	Holocene Alluvial Fan Deposits (*Qhl*)	177
Christchurch	Avon River Floodplain Deposits	442
	Christchurch Formation: Low Energy Deposits	150
	Christchurch Formation: High Energy Deposits	46

map in Fig. 2. The number of CPTs in each evaluated deposit, including in New Zealand, is presented in Table 2. All CPT data are available from the USGS [24].

An innovative aspect of this method is the use of LDI calculated from CPT data representative of each geologic unit and then conversion of LDI distributions to distributions of lateral spread displacement using existing topographic correlations. To do this, free-face ratio and topographic slope are mapped in the Bay Area. Gently sloping areas with slopes less than 5° are easily distinguished by calculating a slope map from the DEM but estimating free-face ratio at regional scales is more difficult. Fig. 3 displays the process of deriving a map of free-face ratio in a portion of the Bay Area around Oakland. Fig. 3a displays a continuous 10-m raster DEM image with terrestrial and bathymetric elevations, and Fig. 3b displays shapefiles of the free-face features and the calculated distance up to 250 m from the free-face features. Then, Fig. 3c displays the resulting estimated heights of the free-face features. The height of a free-face feature was estimated by performing a focal statistics operation whereby the minimum elevation in a 250 m neighborhood around every cell was subtracted from the elevation of the center cell of the moving window. In the last step, free-face ratio, which is displayed in Fig. 3d, was estimated by dividing the distance to the free-face features by the height of the free-face features.

Fig. 4 displays the other model inputs in the Bay area for the back-analysis of the 1989 M_w 6.9 Loma Prieta earthquake. Fig. 4a displays median PGA contours from the USGS ShakeMap [32], Fig. 4b displays a groundwater table model in the Bay Area [26], and Fig. 4c displays locations of observed liquefaction [33].

4.2. *Christchurch, New Zealand Area datasets and uncertainty*

Christchurch CPTs, DEMs, event-specific depth to groundwater models, and liquefaction observations and interpretations are provided in the New Zealand Geotechnical Database (NZGD) [38] and papers by Refs. [39–44]. This study relied primarily on the datasets provided in the NZGD [38] and the Bradley et al. [39] CPT dataset. The DEMs and groundwater models were provided in GIS raster and shapefile formats by Sjoerd van Ballegooy and Nathan McDougall from Tonkin + Taylor [45].

Elevations contained in the 5-m resolution DEMs in the Christchurch area have less uncertainty relative to the USGS 10-m DEMs of the San Francisco Bay Area. Residuals for all DEMs are normally distributed with standard deviations generally on the order of 0.06–0.16 m [46]. For the purposes of this report, uncertainties in the DEM elevations were not considered to investigate their impact on the modeled lateral spread hazard.

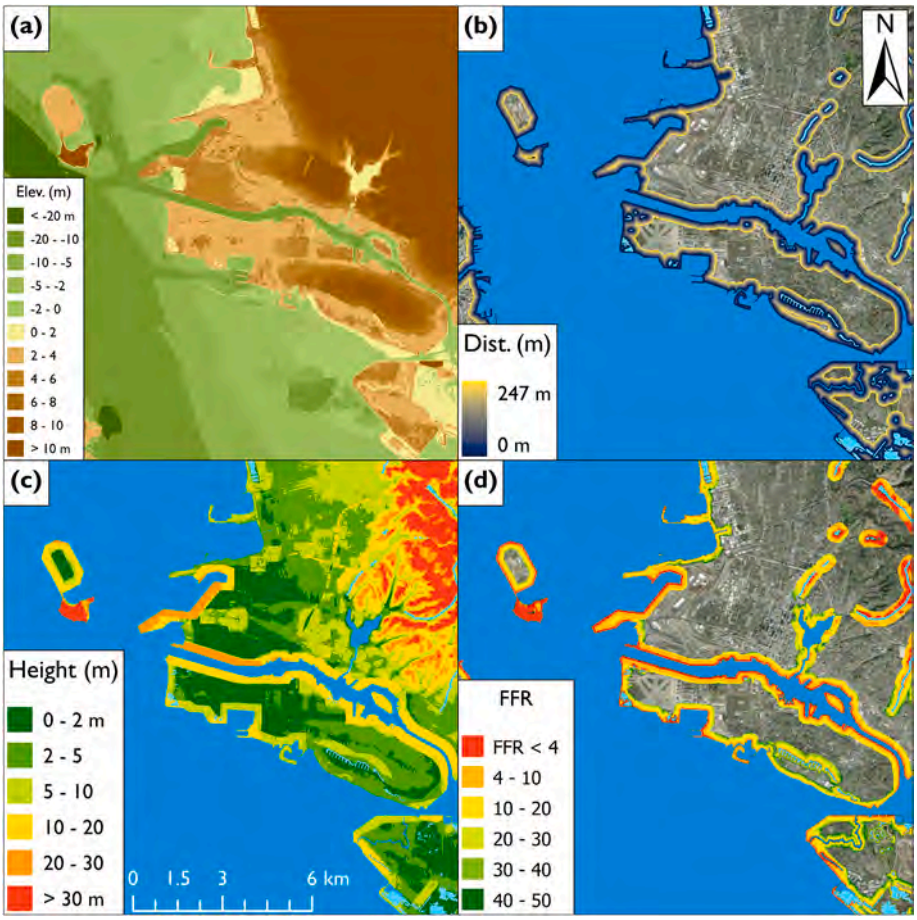

Fig. 3. (color): Process for mapping free-face ratio in Bay Area (a) continuous 10 m resolution DEM with terrestrial and bathymetric elevations, (b) shapefiles of free-face features with calculated distance to features up to 250 m, (c) estimated height of free-face features, and (d) resulting free-face ratio map in Bay Area.

According to van Ballegooy et al. [47], uncertainty in the depth to groundwater models comes predominantly from two sources: temporal fluctuations in groundwater elevations caused by seasonal rainfall, short-term dewatering, or other natural or artificial events, and from geospatial modeling uncertainties from lidar-derived ground surface elevations, errors from interpolation, or errors from other sources. Uncertainty in the depth to groundwater models is geospatially variable and is a function of distance to the nearest monitoring well and the number of readings at that well. Four geospatial classes were created to communicate confidence in the modeled depth-to-groundwater: lowest (west of 4 m median groundwater contour), lower (groundwater table based on widely spread monitoring wells), medium, and higher (groundwater table surface based on closely spread monitoring wells with longer duration monitoring records). Uncertainty in the groundwater table for each of the described uncertainty classes is ±0.5 to ±1.0 m, ±0.4 m, ±0.2 m, and ±0.1 m, respectively. The areas investigated for the purposes of this study are in the medium and higher confidence classes with uncertainty less than ±0.2 m. The uncertainty in the depth to groundwater was not investigated in this study. The sensitivity to the uncertainty in the modeled depth to groundwater is expected to be small given the relatively low values of uncertainty in this dataset.

The western part of the Avon River floodplain was mapped using satellite imagery and LiDAR-based DEMs for this study. This study area was selected because significant lateral spreading was observed during the Darfield and Christchurch earthquakes and although the geology could be refined further, it is generally similar enough within the mapped study area to permit reasonable regional assessments. Regional assessments should not be expected to capture the subsurface geotechnical conditions in as much detail as site-specific assessments. Two additional areas were mapped: a) an area near the coast with Christchurch Formation sands deposited in a high wave energy environment (termed “high energy deposits”) and b) an area adjacent to the high energy deposits, but further inland, with Christchurch Formation sands deposited in a lower energy environment (termed “low energy deposits”). The high energy deposits experienced little to no surface liquefaction during both the Darfield and Christchurch earthquakes and the low energy deposits experienced significant liquefaction. The Avon River floodplain and the NZGD CPTs in that area are shown in Fig. 5.

Free-face ratio in the Avon River floodplain in Christchurch was mapped in a similar manner to the process described previously for the San Francisco Bay Area and illustrated in Fig. 3, except that the free-faces along the Avon River were mapped manually. Additionally, bathymetric data could not be located for the Avon River; therefore, based on cross-sections presented by Robinson [48], it is assumed that the Avon River is a constant 3.5 m depth. As the Avon River is generally between 2 and 5 m depth, use of a constant depth of 3.5 m introduces additional epistemic uncertainty into the analysis.

Fig. 6 displays the median PGA contours and liquefaction severity observations for the Darfield and Christchurch earthquakes in Christchurch. As described by Bradley & Hughes [49], the estimated PGA and uncertainty contours (termed “conditional” PGA and “conditional” uncertainty) were estimated using a New Zealand-specific ground motion model (GMM) and conditioned on observations of ground motion intensity at recording stations. Conditional uncertainty is a function of distance to the nearest recording station; where ground motion is known exactly (i.e., at a recording station), the uncertainty in the shaking intensity is zero and at locations far from a recording station, the uncertainty in the shaking intensity increases to the uncertainty of the New

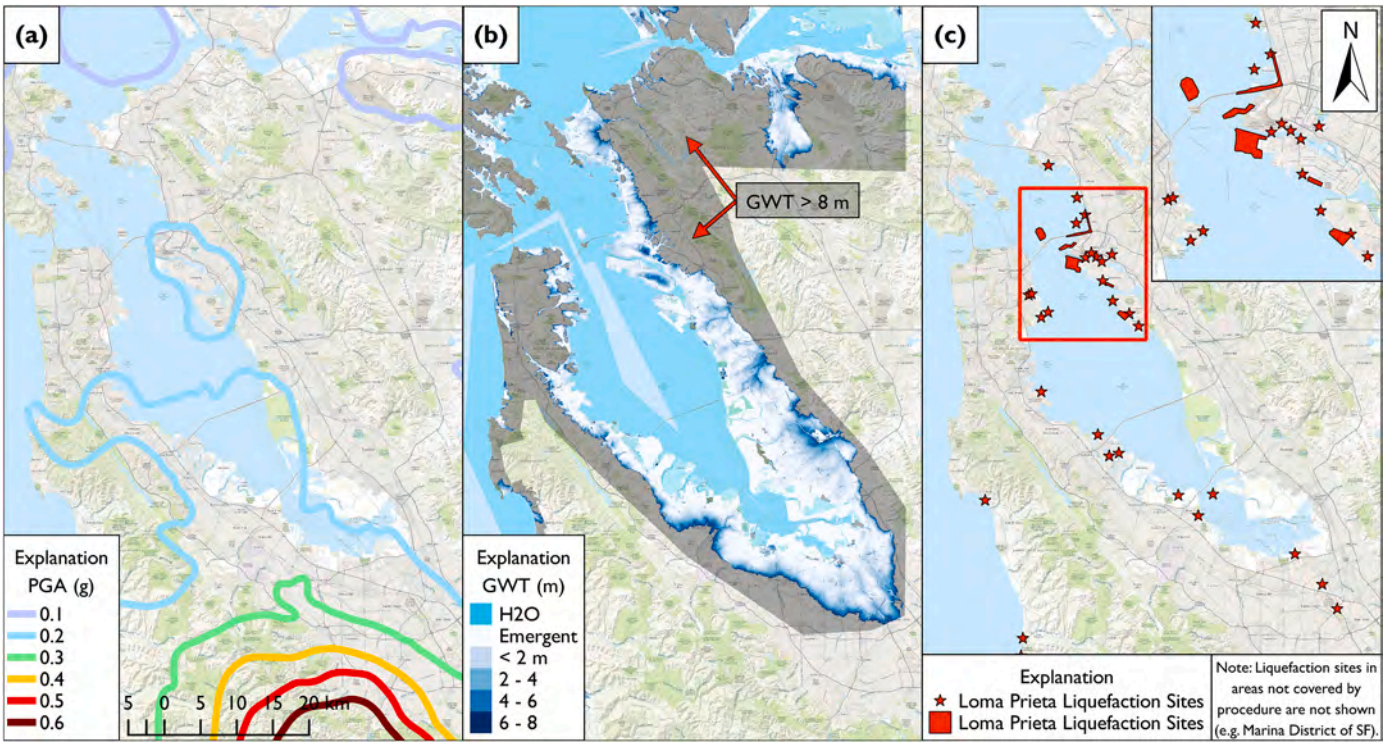

Fig. 4. (color): Datasets in Bay Area for back-analysis of M_w 6.9 Loma Prieta earthquake (a) median PGA contours, (b) GWT model, and (c) locations of observed liquefaction.

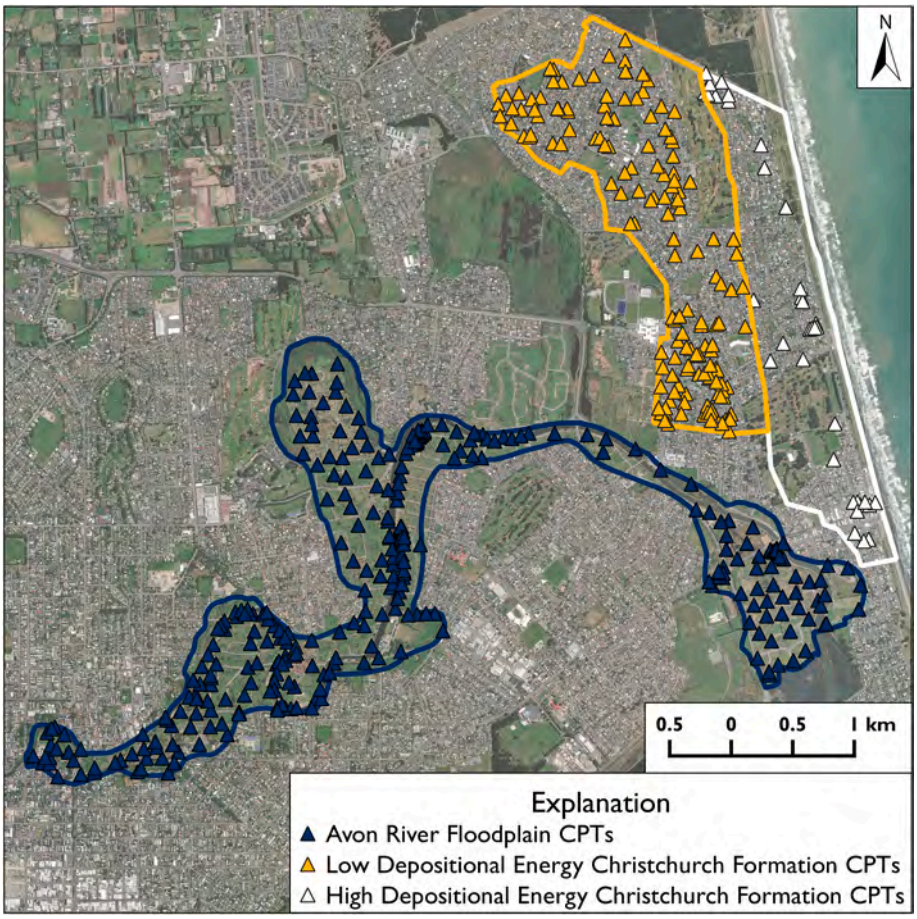

Fig. 5. (color): Investigated regions of Christchurch with locations of NZGD CPTs.

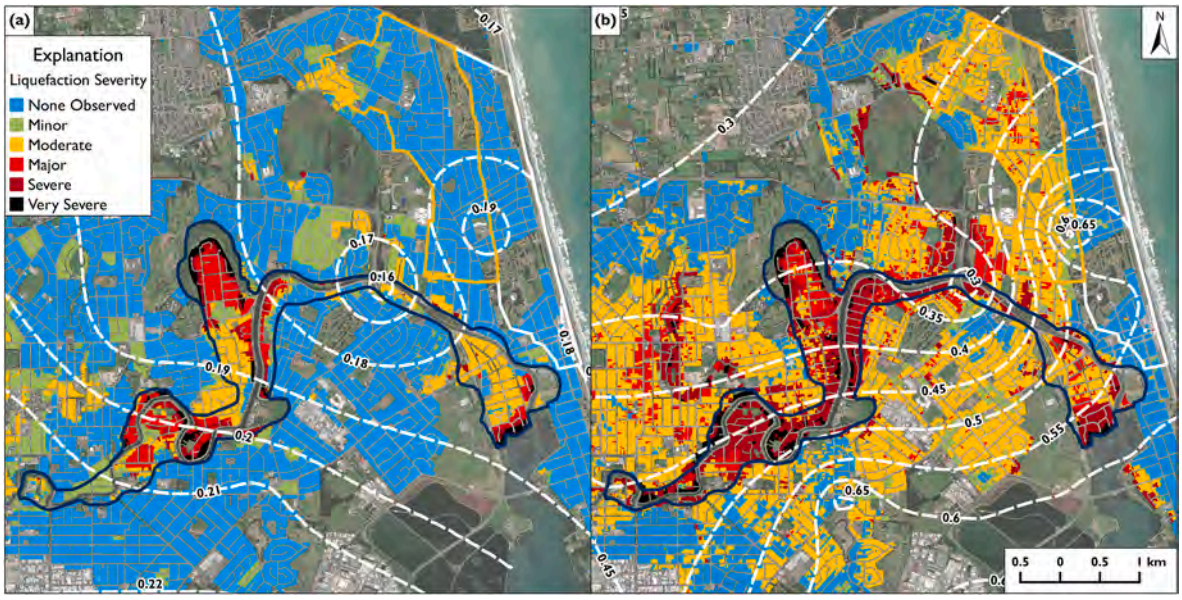

Fig. 6. (color): Conditional median PGA contours and liquefaction severity observations for (a) 2010 M_w 7.1 Darfield earthquake and (b) 2011 M_w 6.2 Christchurch earthquake [49].

Zealand-specific GMM.

5. Model functional form and the mixed random variable distribution

The LDI datasets calculated for each geologic deposit were evaluated to develop models to assess the probability that LDI equals "zero" (i.e., a negligible value), which is delineated as $P_{LDI=0}$. To estimate $P_{LDI=0}$, small values of LDI < 3 were assumed to be essentially zero and the percentage of CPTs with LDI < 3 at each depth to groundwater and each magnitude-scaled PGA was taken to equal $P_{LDI=0}$. The sensitivity of the results to using an LDI threshold of 3 was investigated and found to be minor, as discussed later.

Equation (5a) was fit to the data to estimate $P_{LDI=0}$.

$$Prob_{LDI=0} = 1 - \frac{1 + a_0 * GWT^{a_1}}{[1 + exp[(a_2 + a_3 * GWT) * (PGA/MSF - (a_4 + GWT^{a_5}))]]^{a_6}} \quad (5a)$$

where a_0, a_1, a_2, a_3, a_4, a_5, and a_6 are model fitting coefficients, GWT is the depth to the groundwater table, and the magnitude scaling function (MSF) from Idriss & Boulanger [21]:

$$MSF = 6.9 * exp\left(\frac{-M_w}{4}\right) - 0.058, \; MSF \leq 1.8 \quad (5b)$$

The non-zero LDI data was transformed using the natural logarithm, and Equation (6a) was fit to the data to estimate the mean, non-zero *ln* (LDI).

$$if \; \frac{PGA}{MSF} \leq \left(\frac{PGA}{MSF}\right)_{min} \begin{cases} LDI = 0 \\ else, \ln(LDI) = \dfrac{[b_0 + b_1 * GWT] * \left[\dfrac{PGA}{MSF} - \left(\dfrac{PGA}{MSF}\right)_{min}\right]}{[b_2 + b_3 * GWT] + \left[\dfrac{PGA}{MSF} - \left(\dfrac{PGA}{MSF}\right)_{min}\right]} \end{cases} \quad (6a)$$

where b_0, b_1, b_2, and b_3 are model fitting coefficients, and

$$\left(\frac{PGA}{MSF}\right)_{min} = 0.012 * GWT + 0.06 \quad (6b)$$

The threshold value of $LDI_0 = 3$ was selected after performing an analysis using the dataset calculated from the CPTs available in the *afem* geologic unit in the San Francisco Bay Area. Equation (5a) and Equation (6a) were fit to the data assuming different LDI_0 values of 1, 3, 5, and 10, and the sensitivity of the results to each of these potential threshold values was evaluated. Using the fitted models for the four potential LDI_0 values listed, the median LDI was evaluated for many scenarios consisting of different combinations of PGA, M_w, and GWT and were found to generally have low sensitivity to the selected LDI_0 threshold value.

The residuals for the mean, non-zero *ln*(LDI) models were tested for normality using the Lilliefors test, which is an improvement to the Kolomorgorov-Smirnov (K–S) test. The model residuals for each of the deposits were found to not be normal and were instead fit with skew-normal distributions, which requires shape (α), location (ξ), and scale (ω) fitting parameters. The skew-normal cumulative distribution function (CDF) cannot be solved using closed-form solutions in Excel but is easily solved using programming languages such as Python.

As employed by Bray & Travasarou, Rodriguez-Marek & Song, and Bray & Macedo [50–52], the LDI data are distributed as a mixed random variable. A mixed random variable distribution separates a discrete, lumped mass probability that LDI equals zero from a continuous distribution for non-zero *ln*(LDI) so that meaningless differences in the relative values of low LDI values do not determine the uncertainty in the estimate of meaningful values of LDI when LDI is larger than a selected threshold LDI value (i.e., $LDI_0 = 3$).

6. Geologic based models for San Francisco Bay Area deposits and christchurch, New Zealand deposits

The $P_{LDI=0}$ data and the fit of Equation (5a) to these data and the mean, non-zero *ln*(LDI) data and the fit of Equation (6a) to these data for the *afem*, *Qhly*, and *Qhl* geologic units in the San Francisco Bay Area are shown in Fig. 7. The $P_{LDI=0}$ data and the fit of Equation (5a) to these data and the mean, non-zero *ln*(LDI) data and the fit of Equation (6a) to these data for the Avon River floodplain, and Christchurch Formation low energy and high energy deposits of the Christchurch area are shown in Fig. 8. The model regression coefficients for each of the evaluated deposits are presented in Table 3. Fitting parameters for the skew-normal residual distributions for each of the evaluated deposits are presented in Table 4.

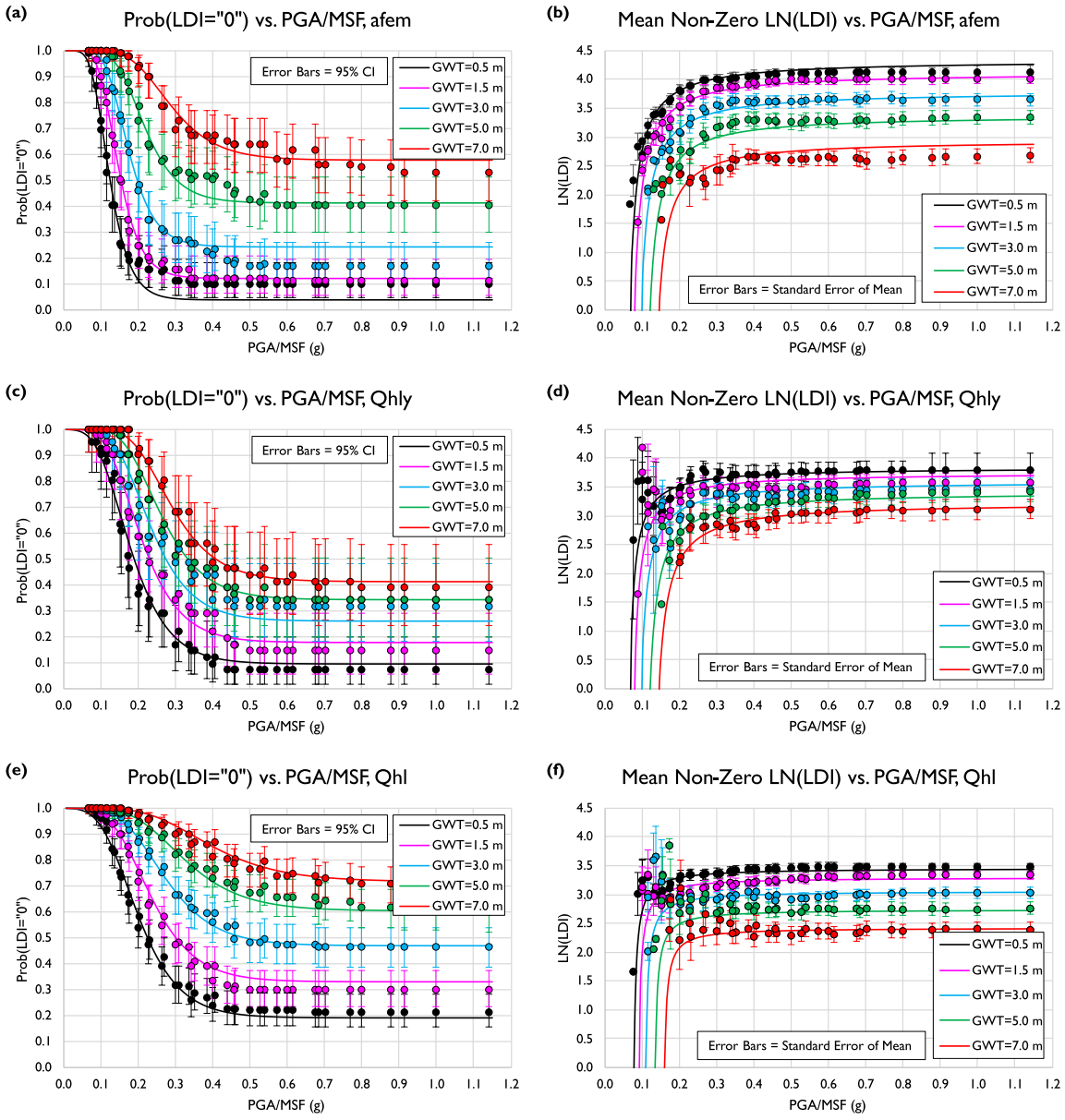

Fig. 7. (color): $Prob_{LDI=0}$ and mean, non-zero *ln*(LDI) models fit to data for: (a) and (b) *afem* deposits, (c) and (d) *Qhly* deposits, and (e) and (f) *Qhl* deposits.

For each geologic deposit, the $P_{LDI=0}$ data show that at low magnitude-scaled PGA values, the $P_{LDI=0}$equals or is close to one, which indicates lateral spread displacement is unlikely (i.e., LDI is likely negligible). The $P_{LDI=0}$ decreases as the magnitude-scaled PGA increases. At large magnitude-scaled PGA values, the $P_{LDI=0}$ asymptotically approaches the percentage of evaluated CPTs within a particular geologic unit with LDI < 3.

The non-zero *ln*(LDI) data show that at magnitude-scaled PGA values less than the minimum magnitude-scaled PGA estimated in Equation (6a), the mean, non-zero *ln*(LDI) equals zero. As the magnitude-scaled PGA increases to an intensity greater than the minimum threshold value estimated for liquefaction triggering and lateral spreading to occur, the mean, non-zero *ln*(LDI) increases quickly before asymptotically approaching the average non-zero *ln*(LDI) value from all evaluated CPTs within a particular geologic unit.

This asymptotic behavior exhibited in both the $P_{LDI=0}$ and non-zero *ln*(LDI) data is mechanistically correct; as the shaking intensity increases, LDI should not increase in an unbounded manner because all saturated, liquefiable soils will eventually liquefy at sufficiently strong ground shaking levels, albeit with low strain potential for dense deposits. The model aleatory variability (inherent randomness) comes from the range of non-zero LDI calculated at each CPT within a particular geologic unit.

7. Conversion of LDI distribution to Lateral Spread Displacement Distribution

The models presented in Figs. 7 and 8 are used to estimate distributions of LDI. An estimated distribution of LDI is converted to a distribution of potential lateral spread displacement using the topographic correlations from Zhang et al. [9] presented as Equations (1) and (2). An example LDI distribution and conversion to a distribution of lateral spread displacement using Equation (2) for Avon River Floodplain deposits and several different values for the free-face ratio is presented as Fig. 9.

To be consistent with the widely used CPT processing software *CLiq*,

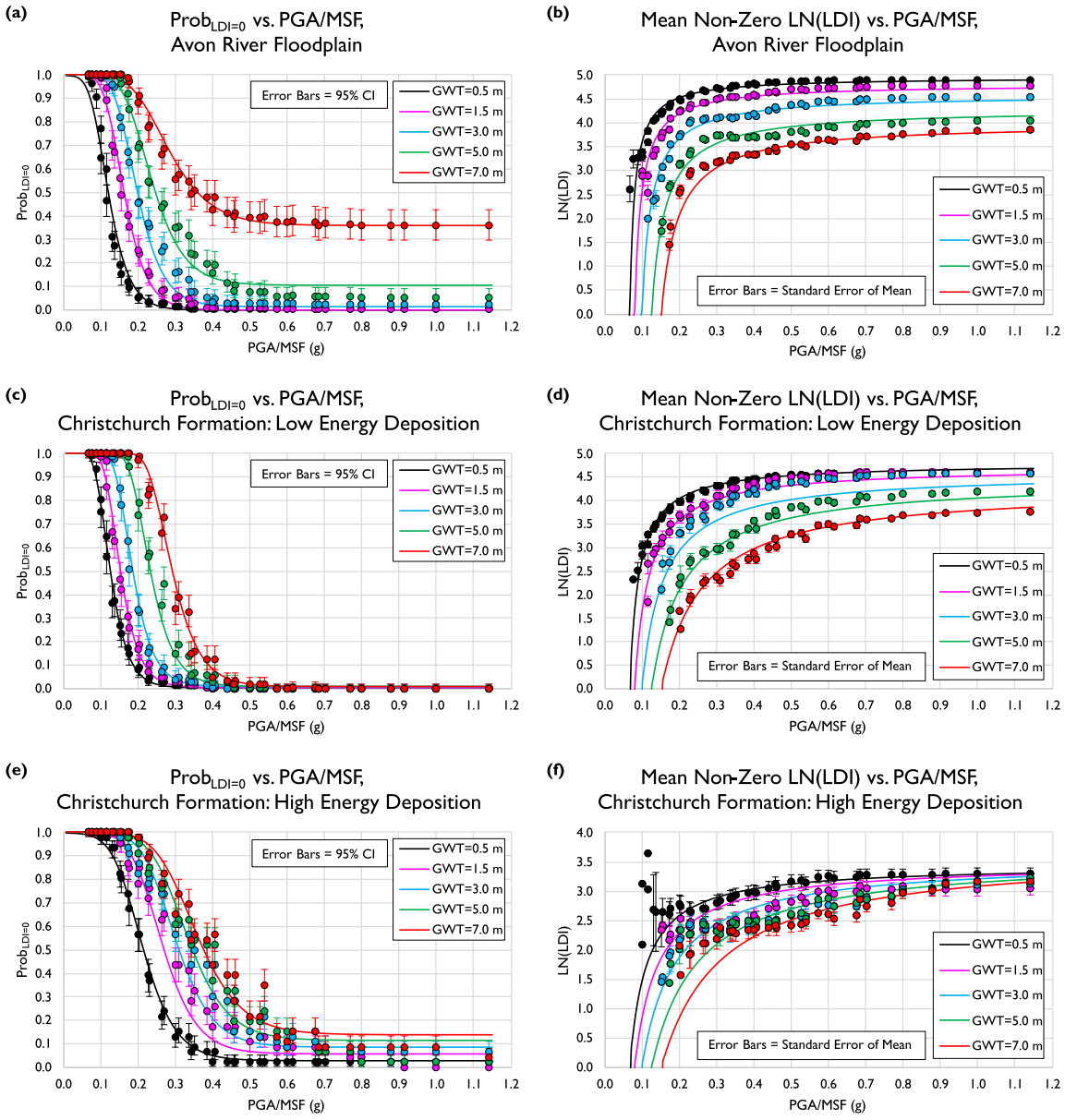

Fig. 8. (color): Prob$_{LDI=0}$ and mean, non-zero *ln*(LDI) models fit to data for: (a) and (b) Avon River Floodplain deposits, (c) and (d) Christchurch Formation: Low Energy deposits, and (e) and (f) Christchurch Formation: High Energy deposits.

the model bounds for Equation (1) are modified from the values presented in Zhang et al. [9] to slopes ranging from 0.1% < S < 5%. Areas far from free-faces with S ≤ 0.1% may experience level ground liquefaction with sand boils and ejecta, but these areas lack sufficient static driving stress to experience lateral spreading. The results are not sensitive to the selection of a threshold value of S = 0.1%. Areas with S ≥ 5% have deposits that are assumed to be too dense to experience lateral spreading. In areas with 3.5% < S < 5%, S = 3.5% is applied in Equation (1) to limit excessive lateral spread displacement estimates.

The model bounds for Equation (2) are expanded in *CLiq* from the values presented in Zhang et al. [9] to *FFR* (L/H) ranges of 1 < *FFR* < 50. This study adopts the increased upper bound of *FFR* = 50, but in areas with 1 < *FFR* ≤ 4, *FFR* = 4 is applied in Equation (2) to limit excessive lateral spread displacement estimates. Lateral spreading due to proximity to a free-face is considered to a maximum of 250 m from a free-face feature.

In areas with gently sloping ground and near a free-face feature with *FFR* < 50, the lateral spread displacement is taken as the maximum value estimated using both the sloping ground displacement estimated from Equation (1) and the free-face displacement estimated from Equation (2). This is advantageous because it is not always clear which condition controls (i.e., sloping ground or free-face). By allowing the model to make this determination automatically, strict, artificial transitions between the two models are avoided.

Liquefaction case histories in California and worldwide indicate that although large areas are often mapped as being susceptible to liquefaction in regional scale studies, only a small proportion of the total land area experiences surface effects of liquefaction and an even smaller proportion experiences lateral spread displacement. In addition to overestimating the spatial extent of surface manifestations of liquefaction, regional assessments also typically overestimate the severity of liquefaction. Even at the site-specific scale, 1-D liquefaction vulnerability indices, such as LPI and LSN, do not capture all of the variables that affect liquefaction severity at the ground surface. For example,

Table 3
Model coefficients for San Francisco Bay Area and Christchurch Area deposits.

Surficial Geologic Deposit	$P_{LDI=0}$ Model Coefficients						
	Parameter						
	a_0	a_1	a_2	a_3	a_4	a_5	a_6
afem	−0.081	1.01	−28.8	2.32	−0.98	0.012	15
Qhly	−0.142	0.55	−14.6	0.34	−1.16	0.018	112
Qhl	−0.270	0.50	−14.0	0.84	−1.01	0.019	13
Avon River	−0.0003	3.63	−29.0	2.15	−0.93	0.033	5.7
Low Energy	−0.005	0.30	−31.9	1.70	−1.11	0.012	1340
High Energy	−0.044	0.59	−19.1	0.73	−0.82	0.045	2.7

Surficial Geologic Deposit	Mean Non-Zero *ln*(LDI) Model Coefficients			
	Parameter			
	b_0	b_1	b_2	b_3
afem	4.43	−0.212	0.018	0.001
Qhly	3.89	−0.096	0.011	0.002
Qhl	3.53	−0.159	0.006	0.0001
Avon River	5.03	−0.148	0.010	0.005
Low Energy	4.83	−0.078	0.018	0.013
High Energy	3.42	0.035	0.035	0.018

Table 4
Skew-normal residuals distribution fitting parameters for San Francisco Bay Area and Christchurch Area deposits.

Surficial Geologic Deposit	Skew-Normal Distribution Fitting Parameters		
	Parameter		
	Shape, α	Location, ξ	Scale, ω
afem	0.00	0.01	0.80
Qhly	−5.72	1.26	1.56
Qhl	1.72	−0.72	1.15
Avon River	−3.88	1.04	1.31
Low Energy	−3.03	0.75	0.93
High Energy	−1.90	0.60	1.02

Hutabarat & Bray [53] studied in-depth 45 sites in Christchurch with and without liquefaction ejecta manifestation. They show that at many of the sites, severe liquefaction manifestation would be predicted using vulnerability indices such as LPI or LSN, but none or only minor manifestation occurred. They found that ejecta manifestation is highly dependent on seepage-induced upward water flow, which is not captured by LPI or LSN. The same is true for the lateral spread hazard; there are many locations where CPTs indicate non-zero LDI and the surface topography is slightly sloping ground or close proximity to a free-face, yet no lateral spreading occurred. In these cases, simplified methods for assessing potential lateral spread displacement do not capture all the variables that affect the potential for and severity of lateral spreading (e.g., spatial continuity of liquefiable layers, and the strength and thickness of the non-liquefied, overlying sediments). For these reasons, the estimated lateral spread displacements are scaled by the proportion of the land area in each unit estimated to be susceptible to liquefaction to limit the overestimation of the liquefaction hazard. Hazus [4] estimates the proportion of land area that is susceptible to liquefaction according to the liquefaction susceptibility class mapped using Youd & Perkins [3] methodology as summarized in Table 5.

Lateral spread displacements estimated using the described procedure are multiplied by the proportion of land area estimated to be susceptible to liquefaction using the values presented in Table 5. Testing of the presented models to estimate LDI and lateral displacements across the study regions without scaling by the factors presented in Table 5 results in significant overestimation of the spatial extent of lateral spreading and the lateral spread severity. In the Bay area, both the *afem* and *Qhly* deposits were estimated by Witter et al. [25] to be very highly susceptible to liquefaction and the *Qhl* deposits were estimated by Ref. [25] to be moderately susceptible to liquefaction. In the Christchurch area, the Avon River Floodplain and the low depositional energy Christchurch Formation sands are estimated to be very highly susceptible to liquefaction and the high depositional energy Christchurch Formation sands are estimated to have low liquefaction susceptibility.

8. Illustrative case history assessments

8.1. San Francisco Bay Area during the 1989 M_w 6.9 Loma Prieta Earthquake

The 1989 M_w 6.9 Loma Prieta earthquake caused significant liquefaction of the sandy artificial fill over estuarine mud (*afem*) deposits along the margins of the San Francisco Bay, especially around Oakland and Alameda, Treasure Island, and the Marina District. Locations of

Table 5
Proportion of land Area susceptible to liquefaction (after [4].

Liquefaction Susceptibility Class	Proportion of Class Susceptible to Liquefaction
Very High	0.25
High	0.20
Moderate	0.10
Low	0.05
Very Low	0.02
None	0.00

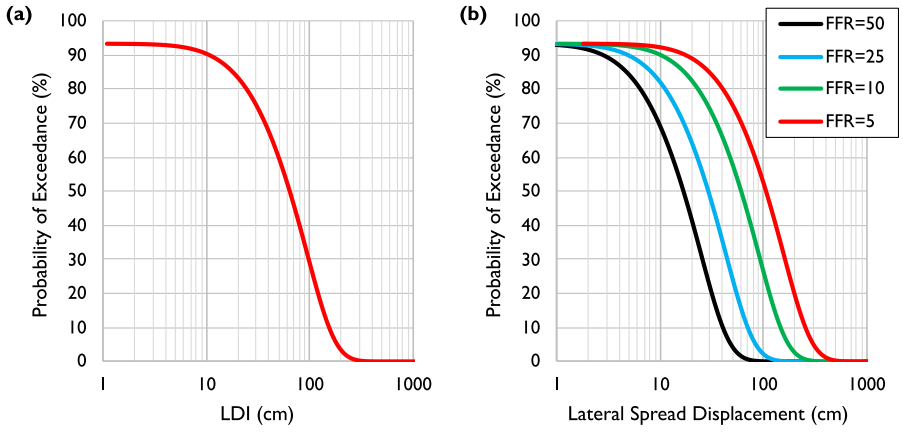

Fig. 9. (color): (a) Example LDI distribution for Avon River Floodplain deposits, GWT = 2.5 m, PGA = 0.41 g, M_w = 6.2 and (b) conversion of LDI distribution to lateral spread displacement distribution for free-face ratios of 50, 25, 10, and 5.

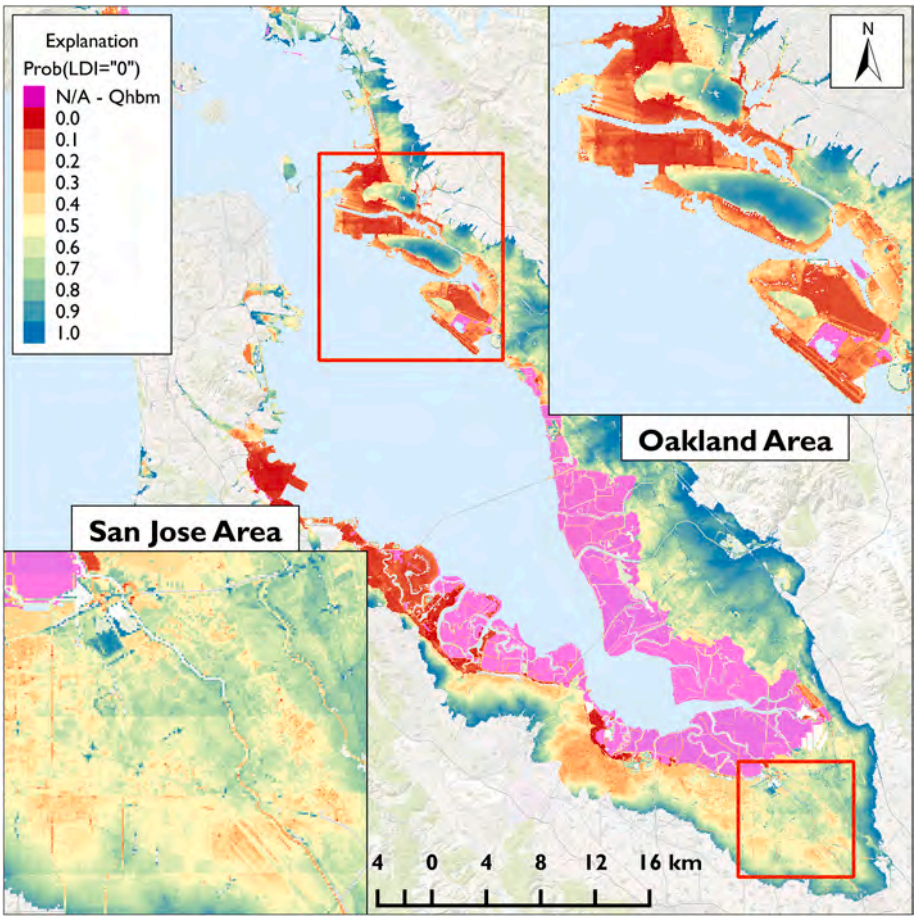

Fig. 10. (color): Modeled $Prob_{LDI=0}$ in the San Francisco Bay Area for the 1989 M_w 6.9 Loma Prieta earthquake.

observed surface effects of liquefaction in the Bay area are presented in Fig. 4c. Lateral spread displacements for the Loma Prieta earthquake were modeled using the proposed procedure with the simplified version of the Witter et al. [25] geologic map presented in Fig. 2, the groundwater table model from the USGS CoSMoS project [26], and the USGS ShakeMap estimates for median PGA [32] shown in Fig. 4a. The study focused on the Oakland and San Jose areas, where the USGS CPT data [24] were available.

Fig. 10 displays the spatial distribution of the estimated $Prob_{LDI=0}$ parameter and Fig. 11 shows the estimated 84%, 50%, and 16% probability of exceedance LDI in the San Francisco Bay Area. This proposed procedure estimates that LDI is highest in the artificial fill deposits around the margins of the Bay and in the youngest Holocene alluvial fan levee deposits in the San Jose area, which is consistent with the observed locations of liquefaction in these areas in the post-earthquake reconnaissance (e.g., Holzer [33]. The proposed procedure estimates the $Prob_{LDI=0}$ to be less than one (though typically greater than 0.5) in the Holocene alluvial deposits. The $Prob_{LDI=0}$ in these areas is higher (i.e., lateral spreading is less likely) compared to the artificial fill and youngest Holocene alluvial fan levee deposits. This is consistent with expectations for these deposits which were mapped as moderately susceptible to liquefaction by Witter et al. [25] compared to very high susceptibility for the artificial fill and youngest Holocene alluvial fan levee deposits. Liquefaction was not observed in the Holocene alluvial fan deposits [33].

Fig. 12 shows the estimated 84%, 50%, and 16% probability of exceedance lateral spread displacements in the Bay Area. At the 50% probability of exceedance level, the proposed procedure estimates the largest lateral displacements near significant free-faces in the artificial fill deposits around the margins of the Bay and in the youngest Holocene alluvial fan levee deposits in the San Jose area near major tributaries such as the Guadalupe River at the 16% probability of exceedance level. Lateral spread displacements estimated as a function of LDI are an index for both the likelihood of liquefaction occurrence and the severity of potential displacements. Estimated lateral spread displacements less than or equal to 5 cm are considered to be negligible, because these areas are unlikely to experience surface manifestations of liquefaction or noticeable lateral spreading. The proposed procedure focuses only on areas where the estimated lateral displacement exceeds 5 cm, which reduces the tendencies for regional scale liquefaction ground failure hazard models to overestimate the spatial distribution and severity of the liquefaction hazard. Comparison of the lateral spread displacement estimates will be discussed further in Section 9 of this paper.

To evaluate the sensitivity to the PGA, the proposed procedure is evaluated in the Bay Area with the 84% and 16% probability of exceedance ground motions. Figs. 13 and 14 show the estimated lateral spread displacements with the 84% and 16% probability of exceedance PGA, respectively. This assessment shows that the estimated spatial extent of lateral spreading and magnitude of displacements decreases significantly with the 84% probability of exceedance PGA as the shaking intensity is insufficient to trigger liquefaction in some areas. The estimated spatial extent and magnitude of displacements increases modestly with the 16% probability of exceedance PGA.

8.2. Christchurch Area during the 2010 M_w 7.1 Darfield and 2011 M_w 6.2 Christchurch Earthquakes

The 2010 M_w 7.1 Darfield and 2011 M_w 6.2 Christchurch earthquakes caused severe, widespread liquefaction in Christchurch, New Zealand with the Christchurch earthquake causing significantly more

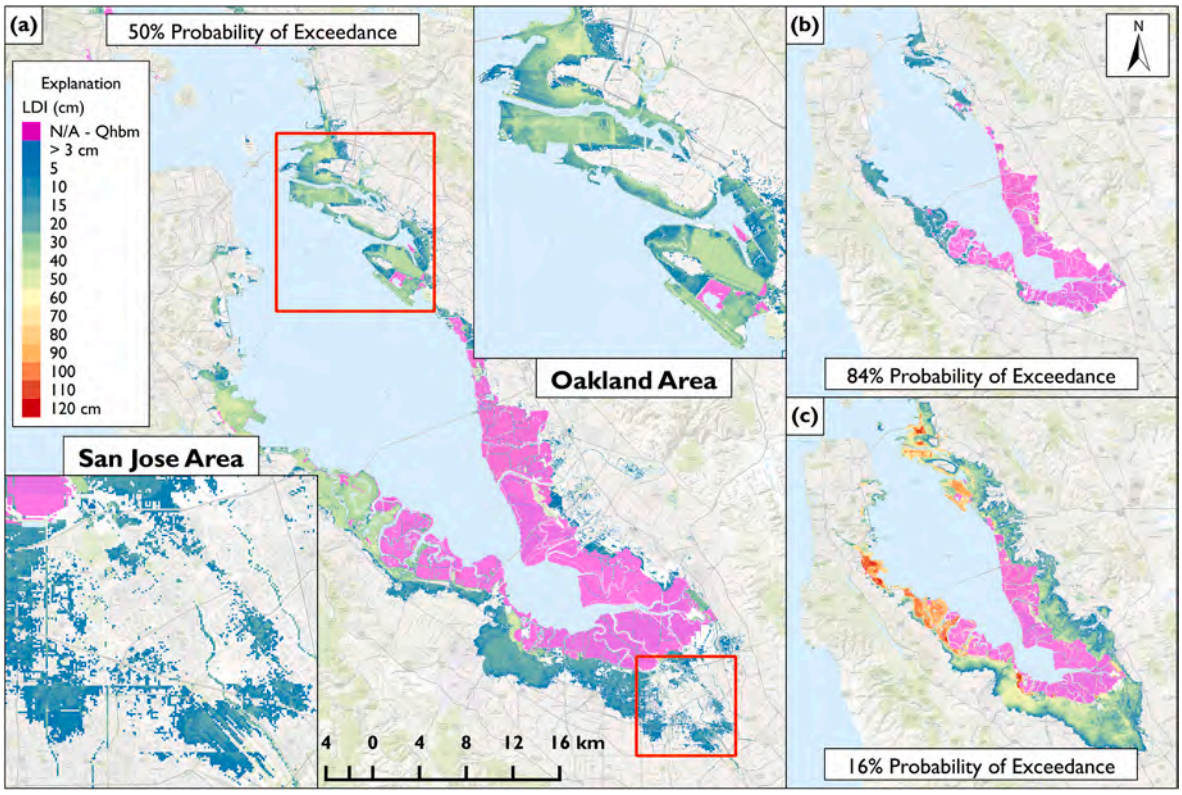

Fig. 11. (color): Modeled LDI in the San Francisco Bay Area for the 1989 M_w 6.9 Loma Prieta earthquake (a) modeled 50% probability of exceedance LDI, (b) modeled 84% probability of exceedance LDI, and (c) modeled 16% probability of exceedance LDI.

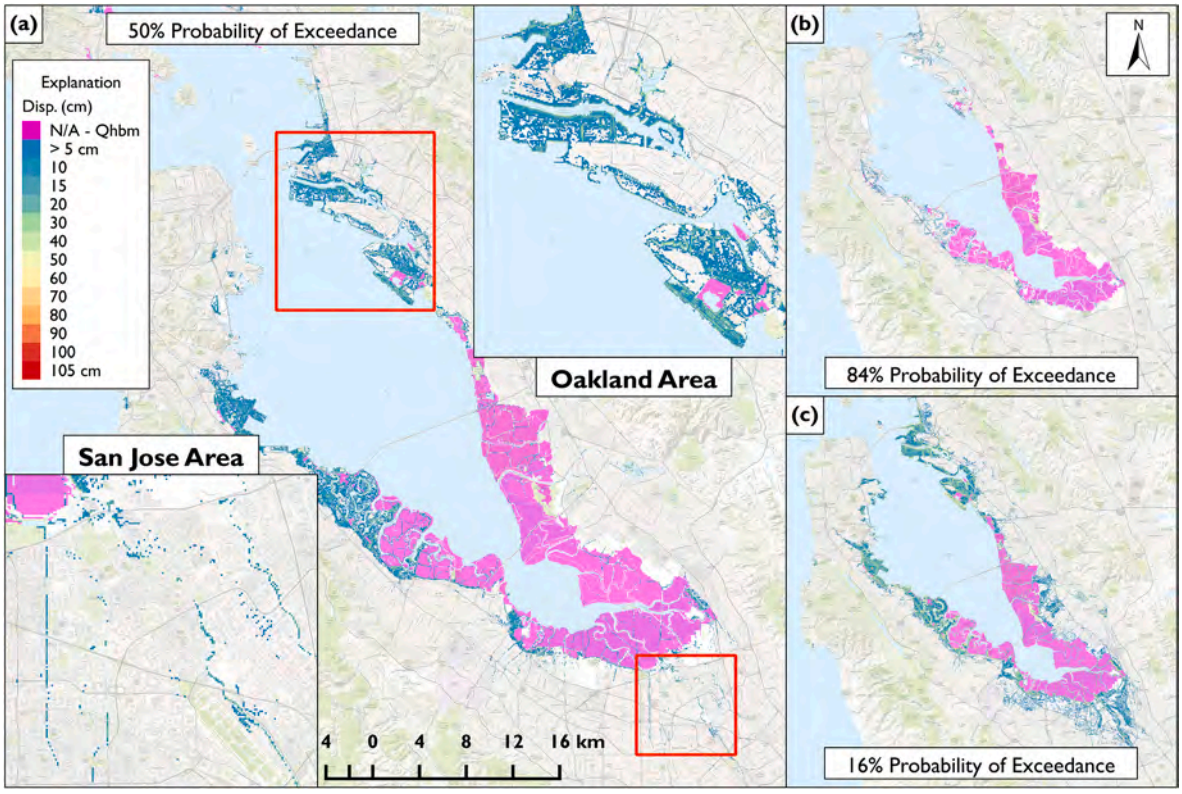

Fig. 12. (color): Modeled lateral spread displacement (LD) in the San Francisco Bay Area for the 1989 M_w 6.9 Loma Prieta earthquake median PGA (a) modeled 50% probability of exceedance LD, (b) modeled 84% probability of exceedance LD, and (c) modeled 16% probability of exceedance LD.

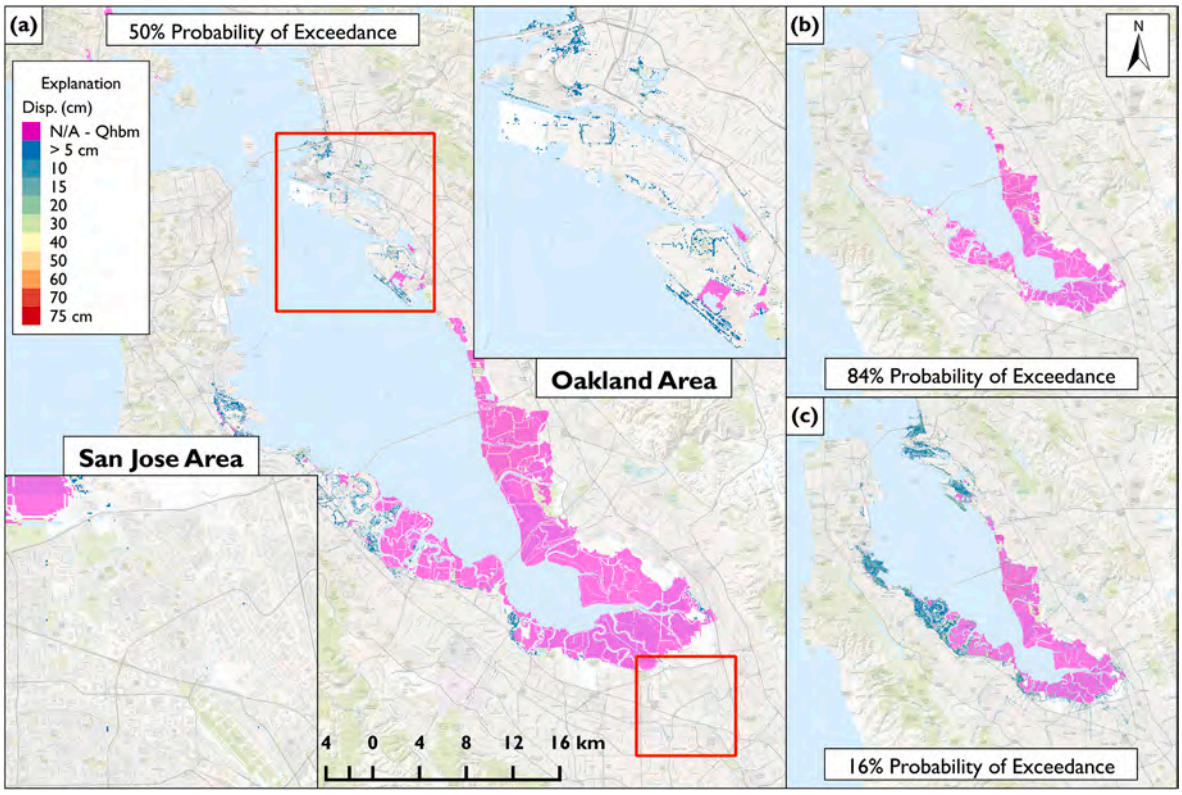

Fig. 13. (color): Modeled lateral spread displacement (LD) in the San Francisco Bay Area for the 1989 M_w 6.9 Loma Prieta earthquake 84% probability of exceedance PGA (a) modeled 50% probability of exceedance LD, (b) modeled 84% probability of exceedance LD, and (c) modeled 16% probability of exceedance LD.

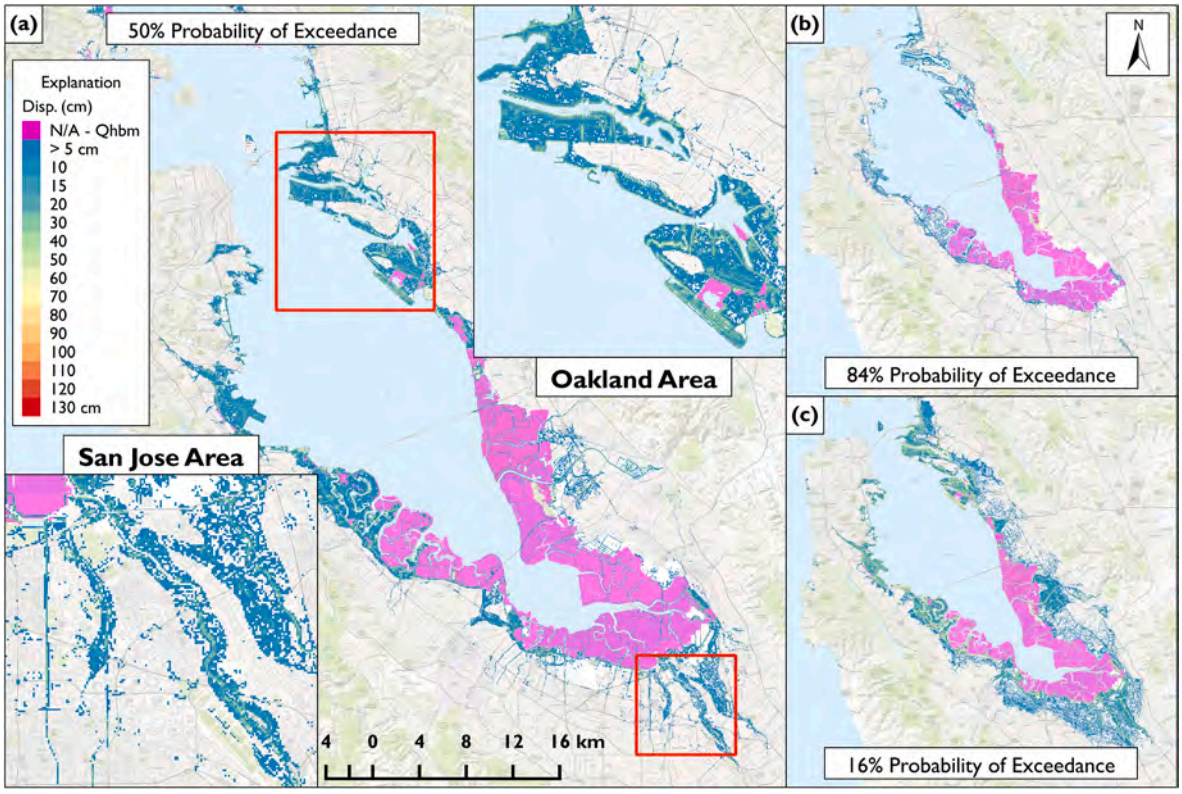

Fig. 14. (color): Modeled lateral spread displacement (LD) in the San Francisco Bay Area for the 1989 M_w 6.9 Loma Prieta earthquake 16% probability of exceedance PGA (a) modeled 50% probability of exceedance LD, (b) modeled 84% probability of exceedance LD, and (c) modeled 16% probability of exceedance LD.

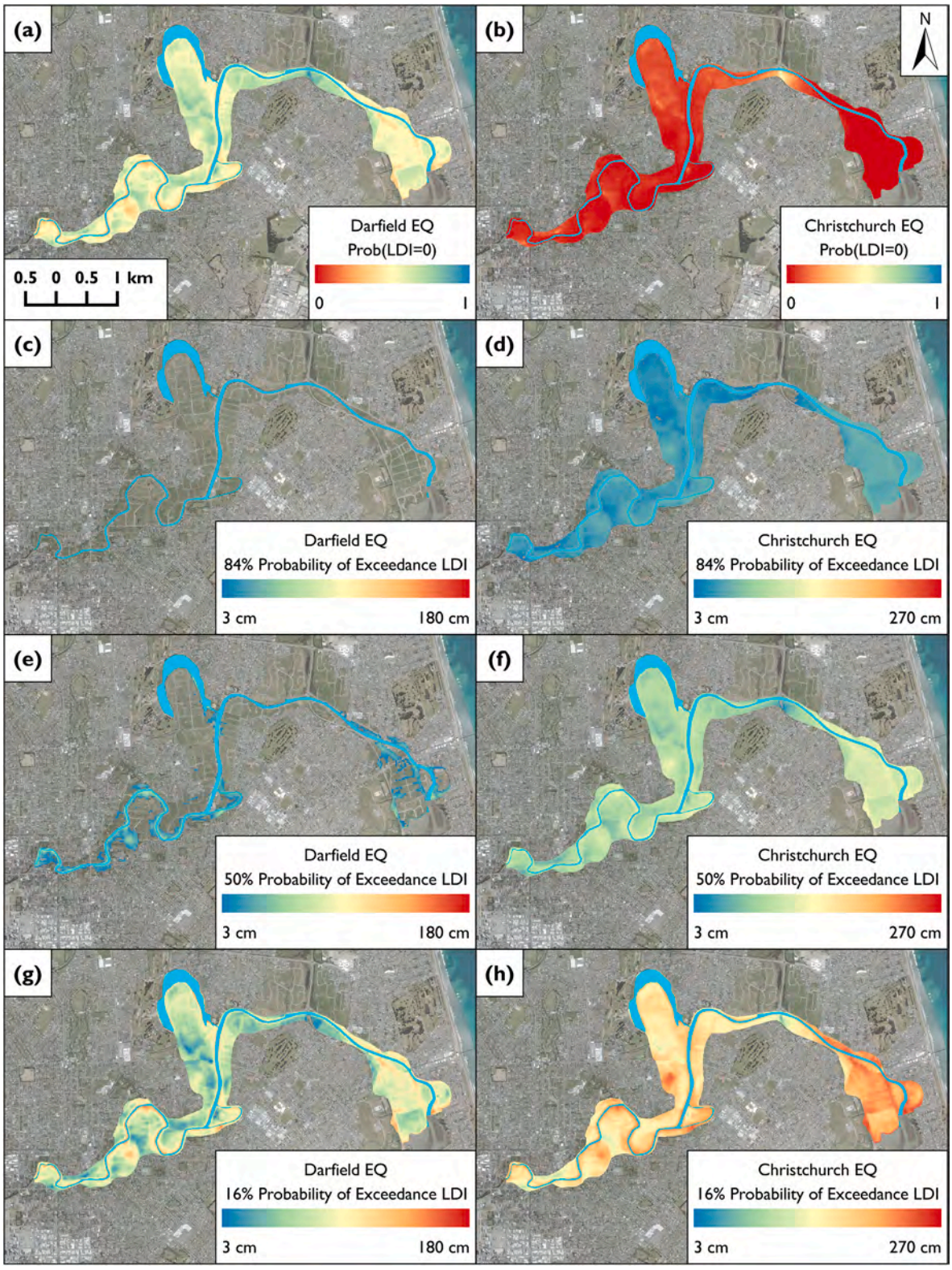

Fig. 15. (color): Avon River Floodplain deposits: (a) $Prob_{LDI=0}$ for the Darfield earthquake, (b) $Prob_{LDI=0}$ for the Darfield earthquake, (c) 84% probability of exceedance LDI for the Darfield earthquake, (d) 84% probability of exceedance LDI for the Christchurch earthquake, (e) 50% probability of exceedance LDI for the Darfield earthquake, (f) 50% probability of exceedance LDI for the Christchurch earthquake, (g) 16% probability of exceedance LDI for the Darfield earthquake, and (h) 16% probability of exceedance LDI for the Christchurch earthquake.

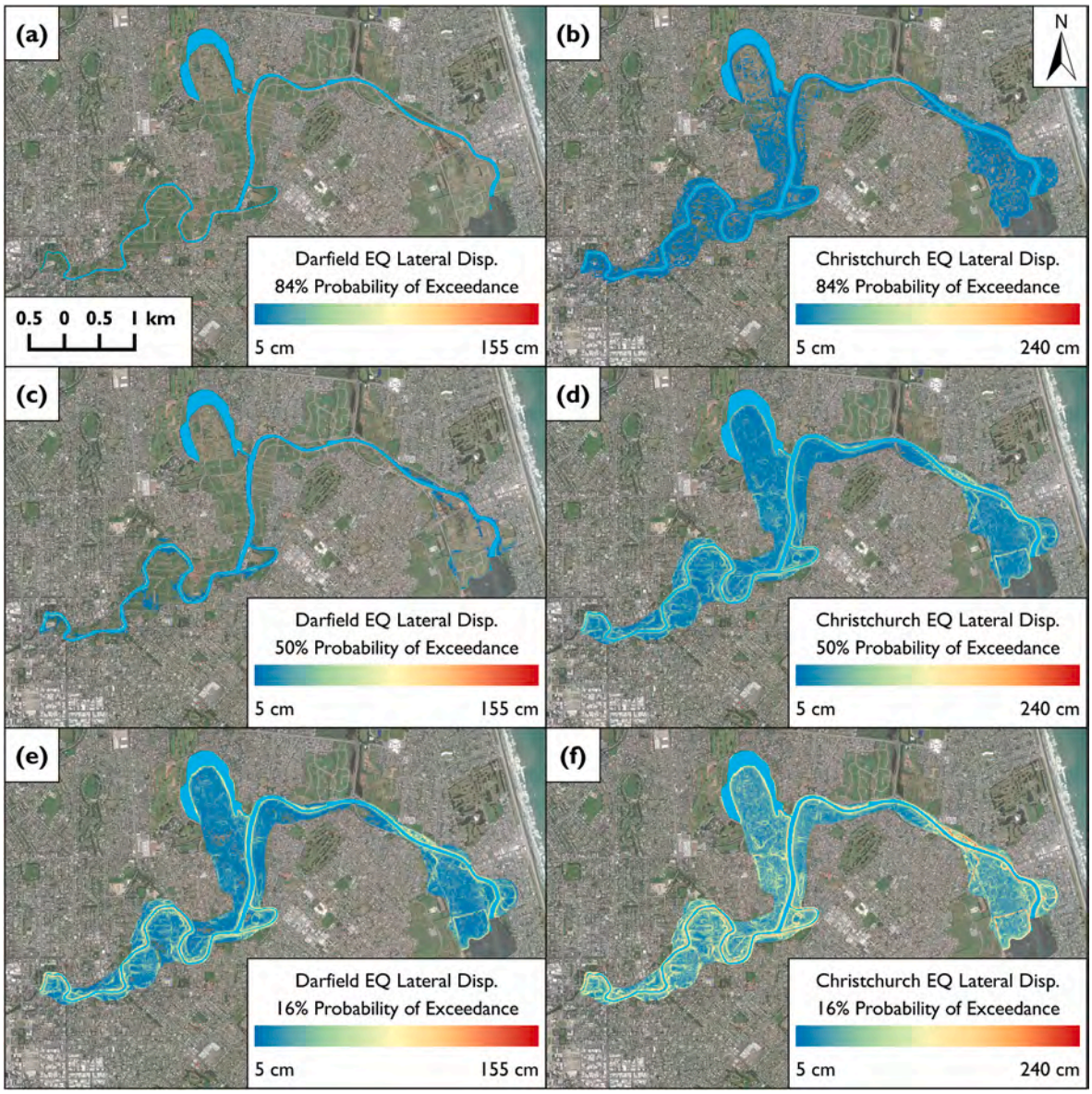

Fig. 16. (color): Avon River Floodplain deposits: (a) Modeled 84% probability of exceedance lateral spread displacement (LD) for the Darfield earthquake, (b) modeled 84% probability of exceedance LD for the Christchurch earthquake, (c) modeled 50% probability of exceedance LD for the Darfield earthquake, (d) modeled 50% probability of exceedance LD for the Christchurch earthquake, (e) modeled 16% probability of exceedance LD for the Darfield earthquake, and (f) modeled 16% probability of exceedance LD for the Christchurch earthquake.

liquefaction-induced damage due to its closer proximity to most of the urban area of Christchurch. Fig. 15 shows the estimated $Prob_{LDI = 0}$ parameter and the 84%, 50%, and 16% probability of exceedance estimated LDI values in the Avon River floodplain deposits for the Darfield and Christchurch earthquakes. This proposed procedure estimates the $Prob_{LDI=0}$ is significantly higher during the Darfield earthquake compared to the Christchurch earthquake, which is consistent with field observations of liquefaction severity (e.g., Refs. [18,38,40,43,44,48]). Correspondingly, the estimated LDI values are much higher for the Christchurch earthquake compared to the Darfield earthquake, which is also consistent with observations [38]. Fig. 16 displays the estimated 84%, 50%, and 16% probability of exceedance lateral spread displacements in the Avon River Floodplain deposits for the Darfield and Christchurch earthquakes, which will be discussed further in Section 9 of the paper.

Fig. 17 displays the estimated $Prob_{LDI=0}$ in the low and high depositional energy Christchurch Formation deposits for the Darfield and Christchurch earthquakes. The $Prob_{LDI=0}$ for the low energy deposits is much lower compared to the high energy deposits and the non-zero LDI is much greater. Correspondingly, the low energy deposits are estimated to have greater LD, as shown in Fig. 18, which is consistent with observations [38].

9. Discussion of illustrative case history assessments

The reasonableness of the lateral spread displacement estimates using the proposed procedure can be quantitatively assessed in the Christchurch area due to the extensive high quality LiDAR ground displacement vectors available [38]. The uncertainty of the LiDAR-derived estimates of lateral spread displacements is generally about twice the uncertainty of the vertical measurements of the LiDAR survey. Most of the areas studied for the purposes of this report have vertical accuracy of ±0.2 m meaning that the LiDAR derived estimates for lateral displacements generally have accuracy of ±0.4 m.

Fig. 19 shows the median estimated lateral spread displacements compared to the measured lateral spread displacements from LiDAR in

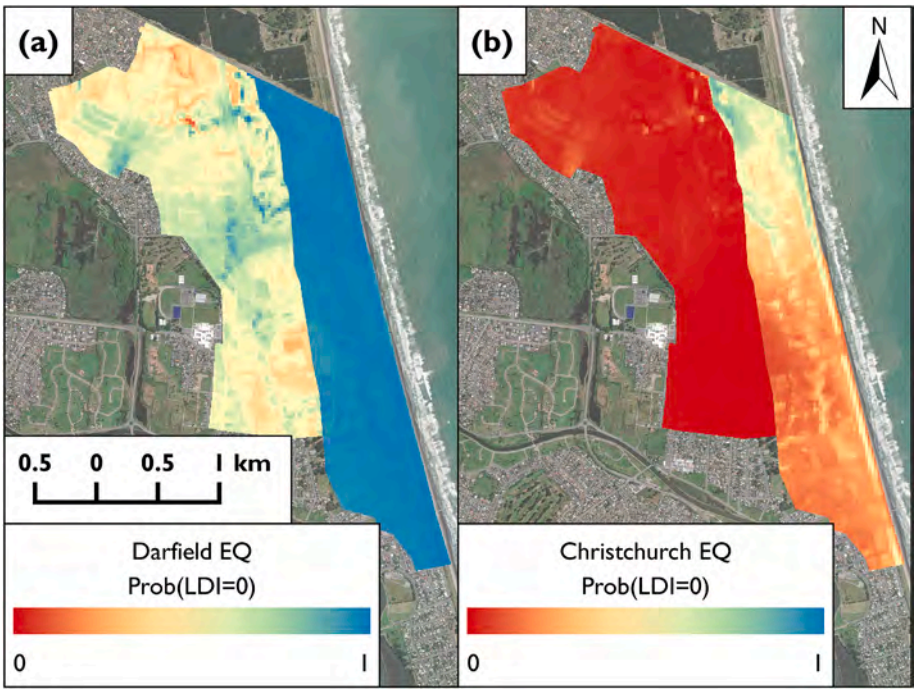

Fig. 17. (color): Modeled $Prob_{LDI=0}$ in the Low and High Energy Christchurch Formation deposits for: (a) Darfield earthquake and (b) Christchurch earthquake.

the Avon River Floodplain deposits and the low depositional energy Christchurch Formation deposits for the Christchurch Earthquake. In the Avon River Floodplain deposits, 62% of median estimated lateral spread displacements for the Christchurch Earthquake are greater than the measured displacements from Lidar indicating the median performance of the proposed procedure is biased slightly high, but the overall magnitude of displacements is captured well for the Christchurch earthquake. Additionally, 54% and 75% of the estimated lateral spread displacements are within a factor of two and within a factor of three, respectively, of the lateral ground displacement measurements from LiDAR. In the low energy deposits, 59% of estimated lateral spread displacements are greater than the measured ground displacements from LiDAR and 48% and 68% of the estimated lateral spread displacements are within a factor of two and within a factor of three, respectively, of the LiDAR ground displacement measurements. The lack of significant LD in the high energy deposits is captured well by the proposed procedure.

In both the Avon River Floodplain deposits and the low energy deposits, the proposed procedure does not capture well the lateral displacements measured from LiDAR during the Darfield Earthquake at the median performance level. The magnitude scaled PGA is near the threshold for liquefaction triggering and the proposed models estimate $P_{LDI=0}$ to be slightly greater than 0.5 (~0.55) in many parts of the evaluated units, leading to zero displacement. The proposed procedure captures the measured lateral displacements from LiDAR well at the 16% probability of exceedance performance level.

In the San Francisco Bay Area, the performance of the proposed procedure is evaluated qualitatively based on the estimated spatial extent of lateral spreading and a comparison of the estimated lateral spread displacements to the reported lateral displacements in select areas. Holzer [33] reports cracks approximately 30 cm wide in the main runway and adjacent taxiway at Oakland International Airport, and he reports 50–70 cm of lateral spread displacement along the west perimeter dike at Oakland International Airport. Additionally, Holzer [33] reports 10-cm wide cracks at the Alameda Naval Air Station, fissures approximately 30 cm wide near the approach to the Bay Bridge, and several meters of lateral spread displacement in the Seventh Street Marine Container Terminal and Matson Terminal at the Port of Oakland where a perimeter dike wall failed. Minor lateral spreading with cracks generally less than 3 cm were reported along Interstate Highway 80, south of the University Avenue exit from Interstate Highway 80 and the frontage road west of the highway [33]. The 84%–16% probability of exceedance range of lateral spread displacements estimated by the proposed procedure in these areas generally capture the observed lateral spread displacement, except for the area where the perimeter dike wall failed. The 84%–16% probability of exceedance lateral spread displacement estimate range underestimates the reported displacement of several meters in this area. Overall, the observed lateral spread displacements in the Oakland/Alameda area are captured reasonably well by the proposed procedure.

Holzer [33] reports that no significant lateral spreading was observed in the San Jose area. Minor lateral spreading resulted in slight ground cracking at the San Jose International Airport along the east bank of the Guadalupe River. No lateral spreading was observed along Coyote Creek. The 84%–16% probability of exceedance modeled lateral spread displacements in these areas generally capture the reported amount and distribution of lateral spread displacements in the San Jose area. Overall, the spatial extent and severity of lateral spread displacements are estimated well in the San Francisco Bay Area.

The performance of the proposed procedure in the Christchurch area and in the San Francisco Bay Area is judged to be good to outstanding for a regional scale liquefaction-induced lateral spread displacement procedure. Both the geospatial extent of lateral spreading and the severity of lateral spreading are estimated reliably for the investigated field case histories. Furthermore, the estimated lateral spread displacements are not biased excessively high or low as demonstrated with the Christchurch earthquake data. Regional scale models tend to overestimate both the spatial extent of liquefaction and liquefaction severity. This is not the case with the proposed procedure.

An analysis by Russell et al. [54] compared the estimated lateral spread displacements using the Zhang et al. [9] method at individual CPTs within approximately the same area of Christchurch of this study and found that 77% of the lateral spread displacement estimates are higher than the displacement measurements for the Christchurch earthquake and 57% of the estimates plot within a factor of two of the displacement measurements. Even when assessing the lateral spread

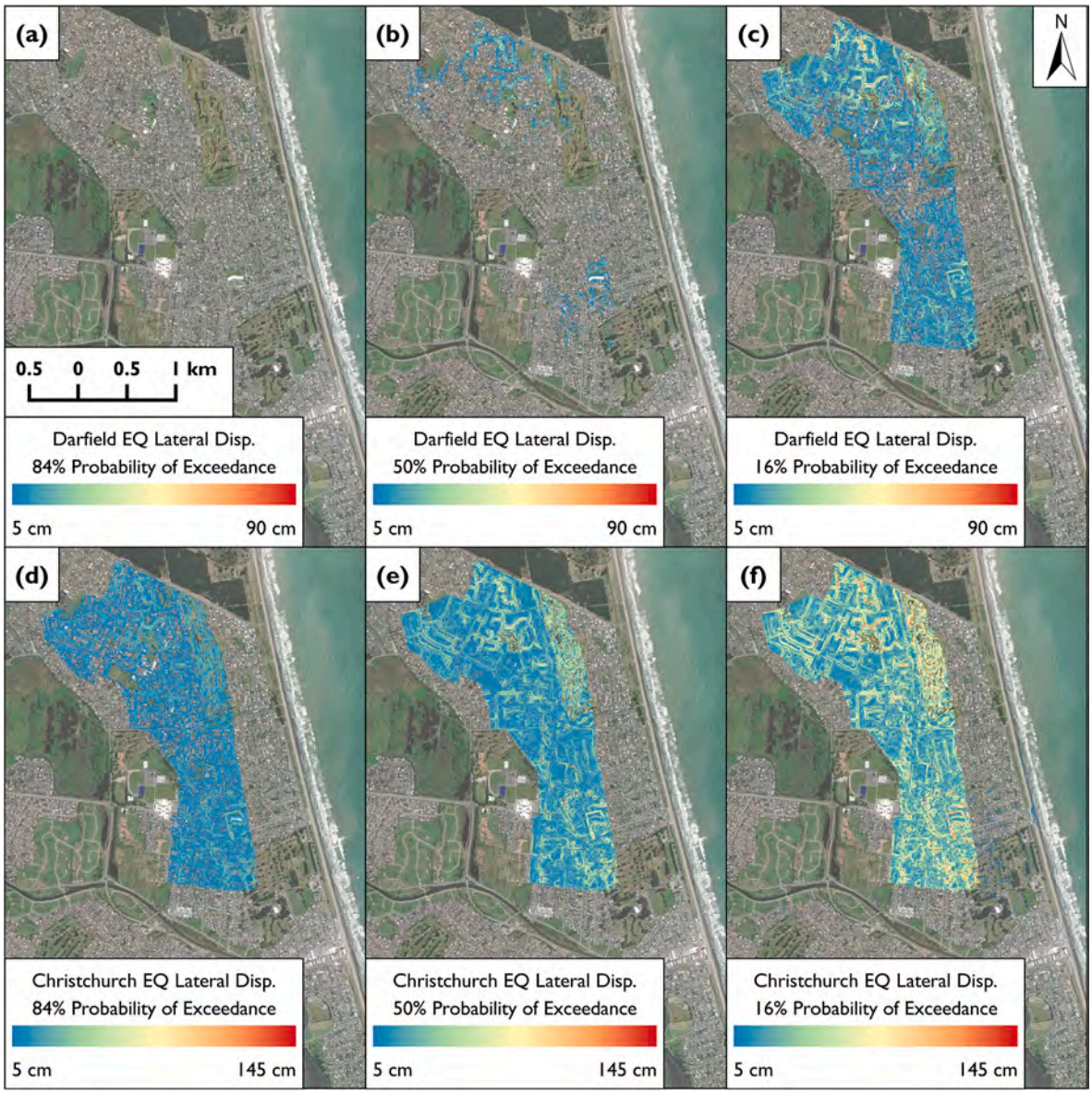

Fig. 18. (color): Low and High Energy Christchurch Formation deposits: (a) modeled 84% probability of exceedance lateral spread displacement (LD) for the Darfield earthquake, (b) modeled 50% probability of exceedance LD for the Darfield earthquake, (c) modeled 16% probability of exceedance LD for the Darfield earthquake, (d) modeled 84% probability of exceedance LD for the Christchurch earthquake, (e) modeled 50% probability of exceedance LD for the Christchurch earthquake, (f) modeled 16% probability of exceedance LD for the Christchurch earthquake.

hazard at individual CPTs, the Russell et al. [54] analysis demonstrates the inherent difficulty in estimating lateral spread displacements using simplified procedures. The performance of the proposed regional scale procedure introduced in this study is about as reliable as the site-specific CPT-based lateral spread procedures widely used in engineering practice. Thus, its performance for the Christchurch earthquake at the regional scale is satisfactory.

10. Limitations

The proposed procedure has several limitations. Firstly, the proposed procedure is only as good as the input geospatial datasets, which all have epistemic uncertainty. GIS-based geologic maps have uncertainty in the accuracy of the linework and in the mapped deposit (i.e., the geologic map may be incorrect). Additionally, surficial geologic maps do not communicate information regarding subsurface conditions, and it is common, especially in alluvial fan environments, for different types of deposits to overlap in the subsurface (e.g., sheet flood deposits may overlap fluvial deposits). Groundwater levels are inherently difficult to map as there is significant uncertainty due to temporal variability in groundwater levels in the rainy season versus the dry season, tidal variations, and local variability due to local groundwater drawdown or recharge and local variations in the hydraulic conductivity of the geologic units. Additionally, long-term climatic trends such as prolonged droughts or a series of exceedingly wet winters will influence the depth to groundwater. Each of these uncertainties vary in time and space and are difficult to assess. Similarly, DEMs have uncertainty from the LiDAR measurements and conversion to bare earth topography.

Another source of uncertainty comes from the way that the free-face ratio is mapped at regional scales. Free-face ratio is defined as the distance to the bottom of the free-face divided by the height of the free-face. To map the free-face ratio in the San Francisco Bay Area and around the Avon River in Christchurch, the lateral distance was estimated to the edge of the free-face features, which likely does not correspond to the location of the bottom of the free-face feature. This systemically underestimates the distance to the free-face feature, resulting in

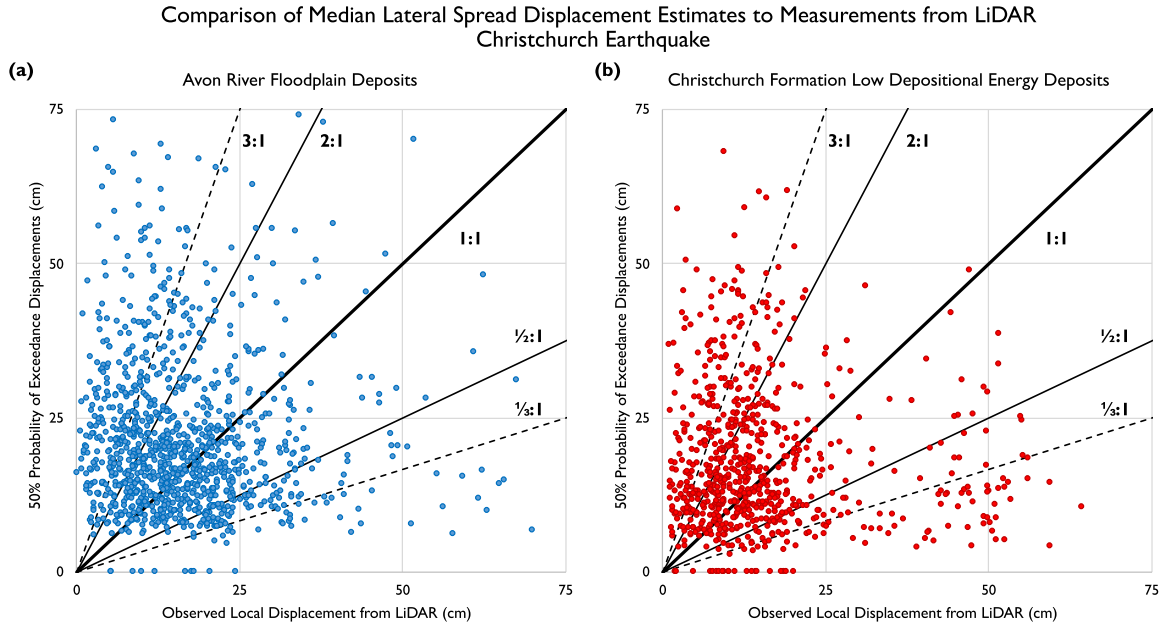

Fig. 19. (color): Comparison of lateral spread displacements measured with lidar from Christchurch earthquake to (a) 50% probability of exceedance lateral spread displacement estimates in the Avon River Floodplain deposits and (b) 50% probability of exceedance lateral spread displacement estimates in the Low Depositional Energy Christchurch Formation sands for median PGA values.

systemically slightly higher free-face ratios. Additionally, the Zhang et al. [9] topographic equations used in the proposed procedure are intended for free-field sites. At regional scales, it is unlikely that sites with free-field conditions can be easily distinguished from sites that have retaining walls or other, non-free-field conditions that buttress the soil and prevent lateral spreading.

Given the limitations associated with evaluating liquefaction-induced lateral spread displacements at regional scales, the method performs well. The highlighted limitations concerning the quality of the input geospatial datasets are in many instances unavoidable, but do not prevent reasonable regional scale assessment of the lateral spread hazard.

11. Conclusions

A new regional scale procedure is presented for probabilistically estimating the lateral spread displacement hazard. The proposed procedure combines subsurface data from CPTs with surficial geologic mapping, groundwater data, the earthquake magnitude, and the earthquake shaking intensity to estimate a distribution of LDI, which is converted to a distribution of lateral spread displacement using the topographic correlations of LDI to lateral displacement presented by Zhang et al. [9].

The proposed procedure produces reasonable results for the 1989 M_w 6.9 Loma Prieta earthquake in the San Francisco Bay Area and the 2010 M_w 7.1 Darfield and 2011 M_w 6.2 Christchurch earthquakes in Christchurch, New Zealand. For both investigated regions, the models estimate reasonably both the spatial extent and severity of liquefaction. In the Christchurch area, the modeling is quantitatively shown to estimate lateral spread displacements in an unbiased manner. Moreover, the median estimate of lateral spread displacement for the Christchurch Earthquake captures most of the measured lateral spread displacement within a factor of two, and this regional scale method performs as well as site-specific CPT-based methods in Christchurch. In the San Francisco Bay Area, the proposed procedure estimates the largest displacements near significant free-faces in the artificial fills along the Bay, particularly in the Oakland/Alameda area, which is consistent with post-earthquake reconnaissance observations.

The proposed procedure advances the state-of-the-practice of regional scale liquefaction and lateral spread displacement modeling through several innovations. Firstly, the proposed procedure capitalizes on the innovative liquefaction probability curves approach developed by Holzer et al. [10]. As discussed, regional scale models typically employ either proxies for geotechnical, geologic, and groundwater conditions (e.g. Zhu et al. [2]- uses V_{S30} as a proxy for geotechnical conditions) or they use kriging techniques to interpolate the liquefaction hazard between widely spaced CPTs or soil exploratory borings. Holzer et al. [10] combined subsurface data from CPTs in the form of the liquefaction potential index (LPI) with surficial geologic mapping, a reliable means for characterizing the liquefaction potential at regional scales [3]. Holzer et al. [10] show that the probability of surface liquefaction can be estimated reasonably as the proportion of CPTs in a geologic unit with LPI > 5 for given PGA, M_w, and GWT.

This study extends the Holzer et al. [10] framework in an innovative manner by characterizing surficial geologic units using the lateral displacement index (LDI), which is commonly used in site-specific methods to estimate lateral spread displacement but has not been used widely in regional scale methods. Models are developed to estimate a distribution of LDI, which are conditioned on surficial geology, PGA, M_w, and GWT. The lateral spread displacement is then estimated based on LDI using topography estimated from DEMs.

Another innovative aspect of this work is how topography is characterized and used in this regional scale procedure. Most lateral spreads occur near a free-face condition and have been characterized by Zhang et al. and Youd et al. [9,13], among others, using the ratio of the distance to the bottom of the free-face to the height of the free-face (i.e., the free-face ratio). As such, to estimate reasonably the locations and severity of lateral spreading at regional scales, it is important to estimate reasonably the free-face ratio of potential lateral spread areas across the region being studied. As illustrated in Fig. 3, the proposed procedure can estimate reliably the free-face ratio using data commonly available over large regions. For example, free-face ratio had not been mapped previously over areas as large as the entirety of the San Francisco Bay Area.

Additional validation studies with the proposed procedure are warranted. For example, the performance of the proposed procedure for other earthquakes, such as the 2014 M_w 6.0 South Napa earthquake,

which produced only limited amounts of minor liquefaction, could be interrogated. The South Napa earthquake produced limited amounts of minor liquefaction in part because it occurred in August at the height of the dry season and it occurred in the midst of a severe, multi-year drought during which groundwater and stream flows were much lower than historical measurements. Additionally, it would be informative to perform forward modeling for several earthquake scenarios in the San Francisco Bay Area. For example, in 2018 the USGS released the results of their *HayWired* study [55], which hypothesized a M_w 7.0 earthquake on the Hayward Fault and modeled the potential ground shaking intensity in the Bay Area. Using the modeled ground shaking intensity, the lateral spread displacement hazard can be estimated and compared if the earthquake occurs during the dry season or the rainy season. Additionally, investigating the effect of potential sea level rise on the lateral spread hazard would be an interesting application of the proposed procedure.

This study demonstrates that liquefaction-induced lateral spreading can be modeled reasonably at regional scales and provides a framework for performing regional scale lateral spread assessments. The San Francisco Bay Area and Christchurch are unique in the quantity and quality of geotechnical, geologic, groundwater, and topographic data that are available. It is hoped that this study motivates organizations to collect the data required to enable the proposed regional scale lateral spread procedure, as well as other procedures, to be performed in other important regions, such as in Los Angeles, Salt Lake City, or Seattle.

CRediT authorship contribution statement

Christopher A. Bain: Conceptualization, Methodology, Writing – original draft.

Jonathan D. Bray: Conceptualization, Methodology, Writing – review and editing, Project Administration, Funding Acquisition.

Declaration of competing interest

The authors declare that they have no known competing financial interests or personal relationships that could have appeared to influence the work reported in this paper.

Data availability

Data will be made available on request.

Acknowledgments

This research was funded by the California Energy Commission (CEC) during the development of the Open Seismic Risk Assessment (*OpenSRA*) software tool. The authors thank the CEC and specifically Yahui Yang, the CEC project manager, for recognizing the importance of this research. Dr. Jennie Watson-Lamprey served as *OpenSRA* project manager for the Pacific Earthquake Engineering Research (PEER) Center team. Professor Thomas D. O'Rourke of Cornell University, Scott Lindvall of Lettis Consultants International, and Dr. Daniel Hutabarat, postdoctoral scholar of UC Berkeley, were vital members of the ground failure research task team and their insights were of great help. The authors also thank Dr. Sjoerd van Ballegooy and Nathan McDougall from Tonkin + Taylor for their thoughtful comments regarding the model development and for providing several important datasets used in the modeling of the Christchurch area.

References

[1] Zhu J, Daley D, Baise LG, Thompson EM, Wald DJ, Knudsen KL. A geospatial liquefaction model for rapid response and loss estimation. Earthq Spectra 2015;31(3):1813–37. https://doi.org/10.1193/121912eqs353m.

[2] Zhu J, Baise LG, Thompson EM. An updated geospatial liquefaction model for global application. Bull Seismol Soc Am 2017;107(3):1365–85. https://doi.org/10.1785/0120160198.

[3] Youd TL, Perkins DM. Mapping liquefaction-induced ground failure potential. J Geotech Eng Div 1978;104(4):433–46.

[4] FEMA. Hazus 4.2 SP3 technical manual. Federal Emergency Management Agency; 2020. https://www.fema.gov/sites/default/files/2020-10/fema_hazus_earthquake_technical_manual_4-2.pdf.

[5] Youd TL, Perkins DM. Mapping of liquefaction severity index. J Geotech Eng 1987;113(11):1374–92. https://doi.org/10.1061/(asce)0733-9410(1987)113:11(1374).

[6] Iwasaki T, Arakawa T, Tokida K. Simplified procedures for assessing soil liquefaction during earthquakes. In: Proceedings of the conference on soil dynamics and earthquake engineering, southampton, UK; 1982. p. 925–39.

[7] van Ballegooy S, Malan P, Lacrosse V, Jacka ME, Cubrinovski M, Bray JD, O'Rourke TD, Crawford SA, Cowan H. Assessment of liquefaction-induced land damage for residential Christchurch. Earthq Spectra 2014;30(1):31–55. https://doi.org/10.1193/031813eqs070m.

[8] Paolella L, Modoni G, Spacagna RL, Baris A. A generalized severity number to predict liquefaction damage with lateral spreading. Geotechnique 2022;1–22. https://doi.org/10.1680/jgeot.21.00006.

[9] Zhang G, Robertson PK, Brachman RWI. Estimating liquefaction-induced lateral displacements using the standard penetration test or cone penetration test. J Geotech Geoenviron Eng 2004;130(8):861–71. https://doi.org/10.1061/(asce)1090-0241(2004)130:8(861).

[10] Holzer TL, Noce TE, Bennett MJ. Liquefaction probability curves for surficial geologic deposits. Environ Eng Geosci 2011;17(1):1–21. https://doi.org/10.2113/gseegeosci.17.1.1.

[11] Youd TL, Idriss IM, Andrus RD, Arango I, Castro G, Christian JT, Dobry R, Finn WD, Harder LF, Hynes ME, Ishihara K, Koester JP, Liao SS, Marcuson WF, Martin GR, Mitchell JK, Moriwaki Y, Power MS, Robertson PK, Stokoe KH. Liquefaction resistance of soils: summary report from the 1996 NCEER and 1998 NCEER/NSF workshops on evaluation of liquefaction resistance of soils. J Geotech Geoenviron Eng 2001;127(10):817–33. https://doi.org/10.1061/(asce)1090-0241(2001)127:10(817).

[12] Toprak S, Holzer TL. Liquefaction potential index: field assessment. J Geotech Geoenviron Eng 2003;129(4):315–22. https://doi.org/10.1061/(asce)1090-0241(2003)129:4(315).

[13] Youd TL, Hansen CM, Bartlett SF. Revised multilinear regression equations for prediction of lateral spread displacement. J Geotech Geoenviron Eng 2002;128(12):1007–17. https://doi.org/10.1061/(asce)1090-0241(2002)128:12(1007).

[14] Faris AT, Seed RB, Kayen RE, Wu J. A semi-empirical model for the estimation of maximum horizontal displacement due to liquefaction-induced lateral spreading. In: Proceedings of the 8th US national conference on earthquake engineering. San Francisco, CA; 2006.

[15] Gillins DT, Bartlett SF. Multilinear regression equations for predicting lateral spread displacement from soil type and cone penetration test data. J Geotech Geoenviron Eng 2014;140(4). https://doi.org/10.1061/(asce)gt.1943-5606.0001051.

[16] Boulanger RW, Idriss IM. CPT-based liquefaction triggering procedure. J Geotech Geoenviron Eng 2016;142(2):04015065. https://doi.org/10.1061/(asce)gt.1943-5606.0001388.

[17] Ku C-S, Juang CH, Chang C-W, Ching J. Probabilistic version of the robertson and wride method for liquefaction evaluation: development and application. Can Geotech J 2012;49(1):27–44. https://doi.org/10.1139/t11-085.

[18] Robertson PK, Wride CE. Evaluating cyclic liquefaction potential using the cone penetration test. Can Geotech J 1998;35(3):442–59. https://doi.org/10.1139/t98-017.

[19] Robertson P. Performance based earthquake design using the CPT. In: Performance-based design in earthquake geotechnical engineering; 2009. https://doi.org/10.1201/noe0415556149.ch1.

[20] Maurer BW, Green RA, van Ballegooy S, Wotherspoon L. Development of region-specific soil behavior type index correlations for evaluating liquefaction hazard in Christchurch, New Zealand. Soil Dynam Earthq Eng 2019;117:96–105. https://doi.org/10.1016/j.soildyn.2018.04.059.

[21] Idriss IM, Boulanger RW. Soil liquefaction during earthquakes. EERI publication. Oakland: Monograph MNO-12, Earthquake Engineering Research Institute; 2008. https://www.eeri.org/.

[22] Jamiolkowski M, Lo Presti DCF, Manassero M. Evaluation of relative density and shear strength of sands from cone penetration test (CPT) and flat dilatometer test (DMT). ASCE Geotechnical Special Publication No. 119; 2001. p. 201–38.

[23] Kulhawy FH, Mayne PW. Manual on estimating soil properties for foundation design. Cornell University. Prepared for Electric Power Research Institute; 1990.

[24] USGS. Map of CPT data: all regions. U.S. Geological Survey; 2020. Retrieved June 1, 2020, from, https://earthquake.usgs.gov/research/cpt/data/.

[25] Witter RC, Knudsen KL, Sowers JM, Wentworth CM, Koehler RD, Randolph CE, Brooks SK, Gans KD. Maps of quaternary deposits and liquefaction susceptibility in the central san Francisco Bay region, California. U.S. Geological Survey Open-File Report 06-1037; 2006. http://pubs.usgs.gov/of/2006/1037/.

[26] USGS. Coastal Storm modeling system (CoSMoS). U.S. Geological Survey; 2021. Retrieved October 1, 2021, from, https://www.usgs.gov/centers/pcmsc/science/cosmos-groundwater#overview.

[27] USGS. MODFLOW 6 modular hydrologic model version 6.3.0. U.S. Geological Survey; 2022. https://doi.org/10.5066/P97FFF9M.

[28] USGS. 3D elevation program 10-meter resolution digital elevation models (published 2020). U.S. Geological Survey; 2020. Retrieved October 1, 2021, from, https://apps.nationalmap.gov/downloader/#/.

[29] Fregoso TA, Wang R-F, Altejevich E, Jaffe BE. San Francisco bay-delta bathymetric/topographic digital elevation model (DEM). U.S. Geological Survey; 2017. https://doi.org/10.5066/F7GH9G27.
[30] San Francisco Estuary Institute and Aquatic Science Center (SFEI ASC). Bay area aquatic resource inventory (BAARI) version 2.1 GIS data. 2017. Retrieved October 1, 2021, from, http://www.sfei.org/data/baari-version-21-gis-data.
[31] Bay Area Open Space Council. Streams: san Francisco Bay area, California, 2008. [Shapefile]. San Francisco Bay Area Upland Habitat Goals Project; 2008. Retrieved October 1, 2021, from, https://maps.princeton.edu/catalog/stanford-km172ps5456.
[32] USGS. M 6.9 – loma Prieta, California earthquake ShakeMap (updated july 7, 2020). U.S. Geological Survey; 2020. Retrieved October 1, 2021, from, https://earthquake.usgs.gov/earthquakes/eventpage/usp00040t8/shakemap/intensity.
[33] Holzer T. The loma Prieta, California, earthquake of october 17, 1989 – liquefaction. 1998. https://doi.org/10.3133/pp1551B. U.S. Geological Survey Professional Paper 1551-B.
[34] Seed RB, Dickenson SE, Idriss IM. Principal geotechnical aspects of the 1989 loma Prieta earthquake. Soils Found 1991;31(1):1–26. https://doi.org/10.3208/sandf1972.31.1.
[35] Befus KM, Barnard PL, Hoover DJ, Finzi Hart JA, Voss CI. Increasing threat of coastal groundwater hazards from sea-level rise in California. Nat Clim Change 2020;10(10):946–52. https://doi.org/10.1038/s41558-020-0874-1.
[36] Wechsler SP. 1999 esri user conference. In: 1999 esri user conference proceedings. Earth Systems Research Institute, Inc.; 1999. Retrieved September 22, 2022, from, https://proceedings.esri.com/library/userconf/proc99/navigate/proceed.htm.
[37] Stoker J, Miller B. The accuracy and consistency of 3D elevation program data: a systematic analysis. Rem Sens 2022;14(4):940. https://doi.org/10.3390/rs14040940.
[38] NZGD. New Zealand geotechnical database. 2021. https://www.nzgd.org.nz/.
[39] Bradley B, Maurer B, Geyin M, Green R, van Ballegooy S. CPT-based liquefaction case histories resulting from the 2010-2016 Canterbury, New Zealand, earthquakes: a curated digital dataset (version 2). 2020. https://doi.org/10.17603/ds2-tygh-ht91. DesignSafe-CI.
[40] Cubrinovski M, Robinson K, Taylor M, Hughes M, Orense R. Lateral spreading and its impacts in urban areas in the 2010–2011 Christchurch earthquakes. N Z J Geol Geophys 2012;55(3):255–69. https://doi.org/10.1080/00288306.2012.699895.
[41] Robinson KM. Liquefaction-induced lateral spreading in the 2010-2011 Canterbury earthquakes (thesis). New Zealand: University of Canterbury; 2016. https://doi.org/10.26021/1749.
[42] Cubrinovski M, Robinson K. Lateral spreading: evidence and interpretation from the 2010–2011 Christchurch earthquakes. Soil Dynam Earthq Eng 2016;91:187–201. https://doi.org/10.1016/j.soildyn.2016.09.045.
[43] Rathje EM, Secara SS, Martin JG, van Ballegooy S, Russell J. Liquefaction-induced horizontal displacements from the Canterbury earthquake sequence in New Zealand measured from remote sensing techniques. Earthq Spectra 2017;33(4):1475–94. https://doi.org/10.1193/080816eqs127m.
[44] Toprak S, Nacaroglu E, Koc AC, O'Rourke TD, Hamada M, Cubrinovski M, van Ballegooy S. Comparison of horizontal ground displacements in avonside area, Christchurch from Air photo, lidar and satellite measurements regarding pipeline damage assessment. Bull Earthq Eng 2018;16(10):4497–514. https://doi.org/10.1007/s10518-018-0317-9.
[45] van Ballegooy S. Personal communication. 2021.
[46] CERA. Verification of LiDAR acquired before and after the Canterbury earthquake sequence. Technical specification 03. In: Canterbury earthquake recovery authority; 2014. Retrieved September 22, 2022, from, https://www.nzgd.org.nz/.
[47] van Ballegooy S, Cox SC, Thurlow C, Rutter HK, Reynolds T, Harrington G, Fraser J, Smith T. Median water table elevation in Christchurch and surrounding area after the 4 september 2010 Darfield earthquake: version 2, GNS science report 2014/18. 2014. April 2014. ISBN 978-1-927278-41-3.
[48] Robinson K, Cubrinovski M, Bradley BA. Lateral spreading displacements from the 2010 Darfield and 2011 Christchurch earthquakes. Int J Geotech Eng 2013;8(4):441–8. https://doi.org/10.1179/1939787913y.0000000032.
[49] Bradley BA, Hughes M. Conditional peak ground accelerations in the Canterbury earthquakes for conventional liquefaction assessment. Technical Report for the Ministry of Business, Innovation and Employment; 2012.
[50] Bray JD, Travasarou T. Simplified procedure for estimating earthquake-induced deviatoric slope displacements. J Geotech Geoenviron Eng 2007;133(4):381–92. https://doi.org/10.1061/(asce)1090-0241(2007)133:4(381).
[51] Rodriguez-Marek A, Song J. Displacement-based probabilistic seismic demand analyses of earth slopes in the near-fault region. Earthq Spectra 2016;32(2):1141–63. https://doi.org/10.1193/042514eqs061m.
[52] Bray JD, Macedo J. Procedure for estimating shear-induced seismic slope displacement for shallow crustal earthquakes. J Geotech Geoenviron Eng 2019;145(12). https://doi.org/10.1061/(asce)gt.1943-5606.0002143.
[53] Hutabarat D, Bray JD. Seismic response characteristics of liquefiable sites with and without sediment ejecta manifestation. J Geotech Geoenviron Eng 2021;147(6). https://doi.org/10.1061/(asce)gt.1943-5606.0002506.
[54] Russell J, van Ballegooy S, Ogden M. Influence of geometric, geologic, geomorphic and subsurface ground conditions on the accuracy of empirical models for prediction of lateral spreading. In: 3rd international conference on performance-based design in earthquake geotechnical engineering; 2017 [Vancouver].
[55] USGS. The HayWired earthquake scenario – earthquake hazards. U.S. Geological Survey; 2017. https://doi.org/10.3133/sir20175013v1. 2017.